Research Square

Preprints are preliminary reports that have not undergone peer review.
They should not be considered conclusive, used to inform clinical practice,
or referenced by the media as validated information.

Implication of Aster-mediated transport and endocytosis in intestinal absorption and human bioavailability of fat-soluble vitamins

Emmanuelle Reboul

Emmanuelle.Reboul@inrae.fr

Aix-Marseille Univ https://orcid.org/0000-0002-4576-1992

Angélique Berthomé

C2VN

Donato Vairo

C2VN https://orcid.org/0000-0002-8771-6524

Marine Chotard

Aix-Marseille Univ

Charles Desmarchelier

Aix-Marseille Univ

Mark Zumaraga

Aix-Marseille Univ

Patrick Borel

Aix-Marseille Univ https://orcid.org/0000-0001-9977-3238

Ángela Bravo-Núñez

C2VN https://orcid.org/0000-0001-5983-5334

Charlotte Sabran

C2VN

Charlène Sirvins

Aix-Marseille Univ https://orcid.org/0009-0006-5947-814X

Article

Keywords:

Posted Date: June 30th, 2026

DOI: https://doi.org/10.21203/rs.3.rs-9607215/v2

License: This work is licensed under a Creative Commons Attribution 4.0 International License.
Read Full License

Additional Declarations: There is **NO** Competing Interest.

Implication of Aster-mediated transport and endocytosis in intestinal absorption and human bioavailability of fat-soluble vitamins

Angélique Berthomé[1], Donato Vairo[1], Marine Chotard[1], Charles Desmarchelier[1,2], Mark Pretzel Zumaraga[1,3], Patrick Borel[1], Ángela Bravo-Núñez[1], Charlotte Sabran[1], Charlène Sirvins[1], Emmanuelle Reboul[1*]

[1]Aix-Marseille University, INRAE, INSERM, C2VN, Marseille, France
[2]Institut Universitaire de France (IUF), France
[3]Department of Science and Technology – Food and Nutrition Research Institute, Bicutan, Taguig, Philippines

*Correspondence: Emmanuelle.Reboul@inrae.fr

SUMMARY

Intracellular trafficking of fat-soluble vitamins in enterocytes remains poorly understood. Recent studies have implicated Aster proteins in the non-vesicular transport of cholesterol and carotenoids from the brush border membrane to the endoplasmic reticulum, alongside an endocytic pathway. Here, we investigated the role of these two pathways in the transport of vitamins A, D, and E. In cultured human intestinal cells, Aster inhibition did not affect retinol esterification, confirming that retinol can reach the endoplasmic reticulum via an Aster-independent pathway. Conversely, Aster inhibition significantly reduced the basolateral secretion of both α-tocopherol and cholecalciferol without altering their uptake. Combined inhibition of Aster and NPC1L1 did not further decrease the secretion of vitamins E and D, indicating a shared pathway. In contrast, dual inhibition of Aster and SR-BI led to an additional reduction in the secretion of vitamins E and D. Inhibition of endocytosis markedly decreased the secretion of vitamins D and E, as well as the esterification of vitamin A. In mice, Aster inhibition lowered vitamin E bioavailability, while in humans, five SNPs in *GRAMD1B* gene correlated with vitamin D bioavailability. This work provides the first evidence of the involvement of Aster proteins and endocytosis in intestinal fat-soluble vitamin absorption.

KEYWORDS
Tocopherol; Cholecalciferol; Retinol; *GRAMD1B*; *GRAMD1C*

INTRODUCTION

Dietary preformed vitamin A (retinol and retinyl esters), D (cholecalciferol and ergocalciferol) and E (tocopherols and tocotrienols) are non-energetic micronutrients required in small amount to support human growth and maintenance. Although their functions differ, their shared hydrophobic nature classifies them collectively as "fat-soluble vitamins"[1]. This common physical trait partly explains why their fate in the digestive tract is linked to that of other dietary lipids. At the end of digestion process, these vitamins in their free or esterified forms are ultimately included in mixed micelles together with other lipid digestion products including free cholesterol. Although other vehicles may exist, incorporation into micellar assemblies enables vitamin uptake at the enterocyte brush border level along the small intestine[2,3]. Several apical-membrane-resident proteins previously identified as cholesterol transport facilitators were recently discovered to participate in fat-soluble vitamin uptake. Vitamin E and D absorption has been demonstrated to be partly facilitated by SR-BI, NPC1L1 and CD36[4,5]. However, the importance of SR-BI in vitamin D intestinal uptake after a 6-week exposure was not confirmed in a SR-BI$^{-/-}$ mouse model[6]. Conversely, vitamin A absorption does not involve these transporters[7], and the way it crosses the brush border membrane is still unclear[8]. Once in the cytosol, the protein CRBPII binds retinol and was proposed to channel it to the endoplasmic reticulum (ER) for esterification[9]. Conversely, how vitamin D and E traffic from the apical membrane to downstream organelles is still unknown[10]. In the ER, retinol is esterified, and retinyl esters together with free vitamin D and E are mainly incorporated into chylomicrons within the Golgi apparatus and then released in the lymphatic circulation. Thus, although part of vitamin fat-soluble absorption process has been unraveled, lack of understanding of specific steps of their transport remains.

Intracellular lipid trafficking is generally governed by both vesicular and non-vesicular transport mechanisms[11].

On the one hand, as for lipids, fat-soluble vitamin transport may be mediated by a non-vesicular (protein-mediated) mechanism[10–13]. This processus can either imply specific proteins like CRBPII for retinol[9], or rely on non-specific associations, for instance with proteins such as fatty-acid binding proteins (FABPs)[14]. Recently, a specific group of proteins, namely Aster -A, -B and -C, encoded by *GRAMD1A*, *-B*, and *-C*, respectively, were described to have a role in the traffic of cholesterol from the plasma membrane to the ER in concert with NPC1L1 and SR-BI in mammalian cells[12,15]. More specifically, knockout or inhibition of both intestinal Asters -B and -C reduced cholesterol esters formation and secretion in mice[16]. Authors also demonstrated that NPC1L1 enriches the plasma membrane with cholesterol, which is necessary for the action of Asters[16]. In agreement with these findings, Bandara and colleagues observed that Aster proteins also facilitate the movement of oxygenated carotenoids (xanthophylls) but not that of the non-oxygenated ones (carotenes), excluding their role in provitamin A transport in the intestine[13,17,18].

On the other hand, several evidences suggest a role of the vesicular endocytosis in cholesterol intestinal uptake. In early 2000s, Hansen and colleagues found SR-BI in clathrin-coated pits in jejunum explants of pigs fed butter[19] and described a quick induction of clathrin-dependent endocytosis in murine intestinal explants submitted to a lipid solution[20]. The main intestinal cholesterol transporter NCP1L1 binds the clathrin-adaptor Numb and recruits clathrin and its adaptor AP2[12,21]. NPC1L1 was also colocalized with cholesterol and endosomal marker EEA1 in murine intestinal cryo-sections[22]. Nonetheless, it remains unclear whether the endocytosis mechanism is directly implied in cholesterol transport itself, similarly to LDL receptor-mediated internalization of LDL[23], or if it participates in the recycling of NPC1L1[12,24]. In contrast, the modest expression of caveolin-1 and scarcity of caveolae in the enterocyte allow to think caveolae/lipid raft-based cholesterol endocytosis is less likely to occur[25]. However, SR-BI is localized in caveolae/lipid raft and impairing its lipid sensing property modifies both raft domain lipid composition and cholesterol distribution in intestinal epithelial cells[26]. Altogether, these data suggest that the functioning of transporter proteins like NPC1L1 or SR-BI could imply a processus of endocytosis for either a direct absorption of molecules like cholesterol, or a sensing/ regulation of cholesterol absorption process. Given the similarities between the digestion - absorption process of cholesterol and vitamins[10,18], we hypothesize that vesicular pathway could also participates in the transport of fat-soluble vitamins[10].

Our aim was thus to assess whether non-vesicular Aster-mediated or endocytosis pathways are involved in vitamins A, D and E intracellular transport in human cultured Caco-2 and in mice. A secondary analysis of a randomized cross-over clinical trial was also conducted to explore the association of genetic polymorphisms in Aster encoding genes with vitamin D and E bioavailability.

RESULTS AND DISCUSSION

Inhibition of Asters by AI-3d reduced α-tocopherol and cholecalciferol secretion but not their intake by Caco-2 TC7 cells

To explore the potential implication of Aster proteins in vitamin A (retinol), vitamin D (cholecalciferol) and vitamin E (α-tocopherol) transport across the enterocyte, we first used differentiated Caco-2 TC7 monolayers grown on filters (**Figure 1A**). In these cells, and as previously reported [16,18], *GRAMD1B* was the predominant transcript (**Figure 1B**). To evaluate Aster involvement, we used the inhibitor AI-3d, which specifically blocks the transfer of cholesterol by Asters[16,27].

We first tested the impact of AI-3d on the intake of retinol, which is esterified at the ER level like cholesterol, using retinol delivered in mixed micelles containing 0.1 mM cholesterol. Indeed, Aster proteins are thought to be recruited and to bind phosphatidylserine in response to the expansion of accessible cholesterol pool in the plasma membrane[16,31], so the presence of micellar cholesterol may be required to promote vitamin transport. We used the reference concentration of 5 μM for AI-3d[16]. No difference in the total vitamin A (retinol + retinyl esters) uptake and the cellular ratio of retinyl esters (sum of retinyl palmitate/ oleate and linoleate) over total vitamin A were noticed between control and AI-3d-inhibited cells after 24h incubation (**Figure 1C**), confirming the data obtained after a 9h-incubation (data not shown). This suggests that retinol targeting to the ER was not Aster-dependent. This is consistent with the fact that a specific cytosolic protein, CRBPII, allows retinol channeling to the ER[9]. This is also in line with the recent publication depicting the Aster-independent uptake and conversion of β-carotene to vitamin A, along with an absence of regulation of *GRAMD1B* by ISX, underscoring the distinct machinery dedicated to vitamin A homeostasis[18].

We then performed experiments with α-tocopherol. We first aimed to determine whether the micellar concentration of vitamin E modulated the effect of AI-3d, as passive diffusion can overpass carrier-mediated transport[10]. To this aim, we addressed the effect of α-tocopherol concentration and Aster inhibition on α-tocopherol uptake and basolateral secretion after a 9h-incubation period (**Figures 1D-F**). α-tocopherol was delivered in mixed micelles containing or not 0.1 mM cholesterol, to evaluate the need of cholesterol presence. These first results showed that, as previously observed, α-tocopherol uptake was decreased in the presence of cholesterol, especially at low tocopherol concentration [4]. There was no effect of AI-3d on α-tocopherol uptake at a concentration of 5μM. However, at α-tocopherol concentrations over 25μM and in presence of 0.1 mM cholesterol, we observed a significant reduction in α-tocopherol secretion. The impact of AI-3d was greater with 0.1 mM micellar cholesterol than without ($p < 0.0001$ vs. $p = 0.0374$, respectively; **Figures 1E-F**). We then further explored the impact of time and AI-3d concentration on α-tocopherol uptake and secretion in a last set of experiments (**Figures 1G-I**). Again, no effect of AI-3d was observed on α-tocopherol uptake. α-tocopherol secretion was higher in the presence of cholesterol (634.8 ± 50.8 vs. 412.4 ± 44.0 pmol in the control condition, at 24h, in presence and absence of cholesterol, respectively). AI-3d concentrations ranging from 1 to 10 μM resulted in significant and dose-proportional reductions in α-tocopherol secretion.

We reconducted this last set of experiments with cholecalciferol. Loading micelles with cholesterol did not impact cholecalciferol uptake (**Figure 1J**). This contrasted with previous results showing that increasing micellar cholesterol could decrease vitamin D uptake[5,32]. However, these previous studies were conducted at low micellar cholecalciferol concentration and for a short incubation time (0.5 μM and 1h, respectively). Again, cholecalciferol secretion was lower in the absence of cholesterol (56.6 ± 7.5 vs. 39.6 ± 1.6 pmol in the control condition at 24h, in presence and absence of cholesterol, respectively). Similarly to α-tocopherol, AI-3d did not impact cholecalciferol uptake in presence or absence of micellar cholesterol (**Figure 1J**), but reduced its secretion over time in a dose-dependent manner ($p = 0.0092$ and $p = 0.0032$, with and without cholesterol respectively, **Figures 1K-L**).

Overall, these experiments showed that Aster inhibition did not impact vitamin E and D uptake, as previously shown for cholesterol[15,16], but that it induced a reduction of both α-tocopherol and cholecalciferol

secretion by Caco-2 TC7 cells (up to -58% for α-tocopherol, and to -50% for cholecalciferol, respectively).

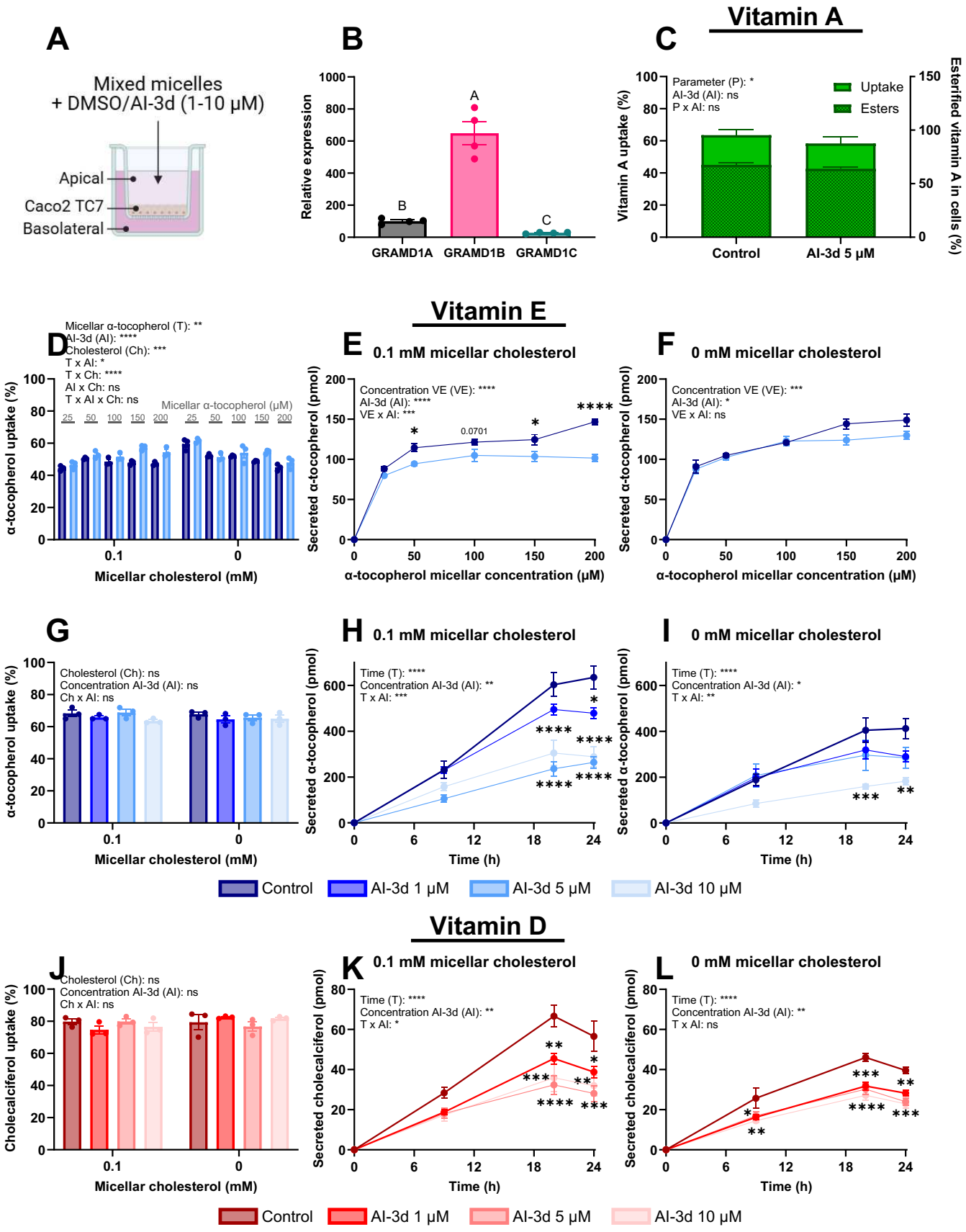


Figure 1: ***Inhibition of Asters by AI-3d reduces α-tocopherol and cholecalciferol secretion but not their uptake by Caco-2 TC7***

(A) Differentiated Caco-2 TC7 on transwells. **(B)** Relative expression of Aster genes in differentiated Caco-2 TC7 monolayers grown on transwells (n=4). **(C)** Vitamin A uptake and esterified vitamin A in cells after a 20h-exposure to micelles containing 5.1 ± 0.1 µM retinol and 0.1 mM cholesterol and 0 (Control) or 5 µM AI-3d (n=4). (**D-F**) Differentiated Caco-2 TC7 were exposed 24h to micelles containing α-tocopherol at 25, 50, 100, 150 or 200 µM (0.1- or 0-mM cholesterol) and 0 (Control) or 5 µM AI-3d (n=3), **(D)** Uptake of α-tocopherol after 9h-exposure, **(E)** Secretion of α-tocopherol in basolateral compartment after 9h-exposure to micelles with cholesterol and **(F)** Secretion of α-tocopherol in basolateral compartment after 9h-exposure to micelles empty of cholesterol. (**G-I**) Differentiated Caco-2 TC7 were exposed 24h to micelles containing α-tocopherol at 67.7 ± 1.2 µM (0.1 mM cholesterol) or 73.3 ± 1.7 µM (0 mM cholesterol) and 0 (Control), 1, 5 or 10 µM AI-3d (n=3), **(G)** Uptake of α-tocopherol after 24h-exposure, **(H)** Secretion of α-tocopherol in basolateral compartment at intermediate (9h and 20h) and end points (24h) after exposure to micelles with cholesterol, **(I)** Secretion of α-tocopherol in basolateral compartment by Caco-2 TC7 at intermediate (9h and 20h) and end points (24h) after exposure to micelles containing α-tocopherol empty of cholesterol. (**J-L**) Differentiated Caco-2 TC7 were exposed 24h to micelles containing cholecalciferol at 8.9 ± 0.1 µM (0.1 mM cholesterol) or 9.0 ± 0.1 M (0 mM cholesterol) and 0 (Control), 1, 5 or 10 µM AI-3d (n=3), **(J)** Uptake of cholecalciferol after 24h-exposure, **(K)** Secretion of cholecalciferol in basolateral compartment at intermediate (9h and 20h) and end points (24h) after exposure to micelles with cholesterol, **(L)** Secretion of cholecalciferol in basolateral compartment at intermediate (9h and 20h) and end point (24h) after exposure to micelles empty of cholesterol. Data are presented as means ± SEM. Geisser-Greenhouse corrected Repeated Measures One-way ANOVA with Tukey's multiple comparison test for B. Two-way ANOVA for E, F, G and J with Šidák's multiple comparison test for E and F. Geisser-Greenhouse corrected Repeated Measures Two-way ANOVA with Dunnett's multiple comparison test for H, I, K and L. Three-way ANOVA for D. *p < 0.05, **p < 0.01, ***p < 0.001 and ****p < 0.0001 compared to Control (AI-3d 0µM). Distinct letters indicate significant differences (p < 0.05). For L, asterisks for AI-3d 1 µM and AI-3d 5 µM are the same for t=9h and 20h (*p and **p respectively), and for t=24h asterisks are the same for AI-3d 5 µM and AI-3d 10 µM (***p).

These results present initial observations of the involvement of Aster in vitamin D and E trafficking in Caco-2 cells. Besides, one of the principal feature of Aster proteins that has been depicted so far is to localize to the plasma membrane based on the level of membrane cholesterol[15]. In the enterocyte, NPC1L1 binds micellar cholesterol to expand the plasma membrane accessible pool[12,16]. Our data support that the presence of micellar cholesterol can likely promote Aster recruitment but is not necessary to allow vitamin D and E transport via Aster proteins. Therefore, this suggests that micellar lipids, including α-tocopherol and cholecalciferol, are likely able to provoke arrangement in the membrane bilayer in a way that lead to the binding of Aster protein GRAM-domain to plasma membrane phosphatidylserine[15].

AI-3d reduced γ-tocopherol postprandial plasma response and liver γ-tocopherol accumulation in mice

Given the significant diminution of both α-tocopherol and cholecalciferol basolateral secretions induced by AI-3d in Caco-2 TC7 cells, we explored whether vitamin postprandial responses after an oral gavage would be affected in a similar way by AI-3d 10 mg/kg in mice. This dose previously led to significant reduction of cholesterol *in vivo* secretion[16]. Two independent postprandial experiments were carried out with either γ-tocopherol or cholecalciferol at dietary doses, as calculated based on body surface area factor[33] (**Figure 2A**). γ-tocopherol was chosen over α-tocopherol because it is a better tracer for vitamin E postprandial absorption [35,36]. An additional experiment was performed with cholecalciferol at a pharmacological dose, as it was shown that cholecalciferol postprandial response could be differently impacted depending on the oral dose provided to mice[34].

AI-3d oral delivery to animals for 2 days prior experiment did not impact body and liver weights or intestinal length (**Figure S1A-C**). No difference in intestinal vitamin content was observed at the end of the postprandial phase (**Figures 2B-C and 2I-J**), which was consistent with the absence of impact of the inhibitor on vitamin uptake in Caco-2 TC7. Both γ-tocopherol and cholecalciferol accumulated gradually along the small intestine, similarly to triglycerides but not to cholesterol (**Figures S1D and S1E**). Postprandial plasma responses for dietary doses of γ-tocopherol and cholecalciferol tended to be lower over time ($p = 0.0583$ and $p = 0.0899$, respectively; **Figures 2C-D and 2J-K**) in the AI-3d-treated group compared to the control group. Inhibitor impact was significant after correcting postprandial vitamin curve for postprandial plasma lipids in the case of γ-tocopherol but not in the case of cholecalciferol (**Figures 1F-G and 1M-N**). Finaly, hepatic γ-tocopherol amount was lower in AI-3d group compared to control ($p= 0.0192$; **Figure 2H**), while no difference was observed for cholecalciferol (**Figure 2O**). Cholecalciferol being hydroxylated in calcifediol in the liver, we looked at liver and plasma calcifediol, which remained globally unaffected (**Figures S2N and S2O**). At pharmacological dose of cholecalciferol, no difference was

observed between control and AI-3d groups, except in the liver (**Figure S1F-L**), which is consistent with a previous study showing that such high concentration can mask the effect of treatment [34].

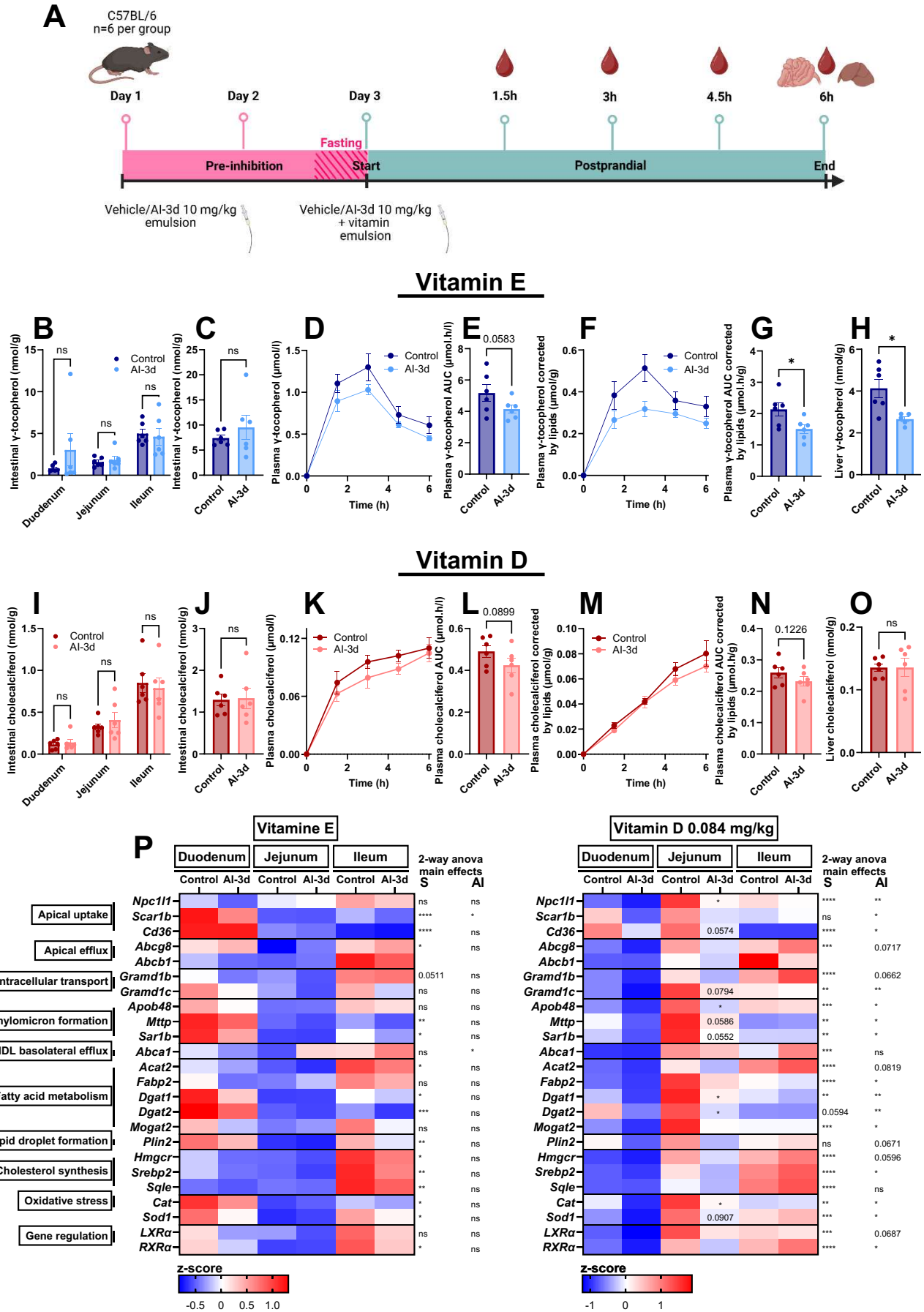


Figure 2: ***Inhibition of Asters by AI-3d tends to reduces γ-tocopherol and cholecalciferol postprandial plasma responses at dietary doses***

(A) Experimental design of the 3 independent postprandial experiments in C57BL/6 male mice. 12 mice were administrated 10 mL/kg emulsion loaded with 15 mg/kg γ-tocopherol alone (Control, n=6) or supplemented with AI-3d 10 mg/kg (AI-3d, n=6). **(B)** γ-tocopherol in intestinal segments at the end of the postprandial phase; **(C)** γ-tocopherol total intestinal content; **(D)** Plasma γ-tocopherol was monitored up to 6h after force-feeding; **(E)** area under the curve of γ-tocopherol postprandial responses; **(F)** Plasma γ-tocopherol corrected by plasma lipids (triglycerides + cholesterol), **(G)** Area under the curve of γ-tocopherol postprandial responses after correction by lipids; **(H)** Hepatic γ-tocopherol measured at the end of the postprandial phase. Panels **(I)**, **(J)**, **(K)**, **(L)**, **(M)**, **(N)** and (**O)** correspond respectively to panels (B), (C), (D), (E), (F), (G) and (H) for cholecalciferol administrated at 0.084 mg/kg. **(P)** Gene expression z-scores in intestinal segments for each independent experiment described above.

Data are expressed as means ± SEM. For each independent experiment, and each gene for P, Geisser-Greenhouse corrected Repeated Measures Two-way ANOVA for B, D, F, I, K, M and P with Šidák's correction for multiple comparison test between Control and AI-3d groups. Unpaired two-tailed t-test for C, H, J and O and one-tailed t-test for E, G, L and N, with Welch's correction when necessary. For (H), one outlier in AI-3d group was identified with ROUT method (Q =1%) and was thus removed from the analysis. Ns non-significant, *p < 0.05, **p < 0.01, ***p < 0.001 and ****p < 0.0001. For panel P, are reported p-values associated with main effects of Intestinal Segment (S) and Control or AI-3d Groups (AI), no significant interaction was detected for each gene in each experiment. Asterisks or values close to *p < 0.05 significance reported in the Heatmap corresponds to differences between Control and AI-3d Group in one segment.

To assess whether AI-3d treatment, and the combination with vitamin E or D force-feeding, induced modulations that would interfere with Aster inhibition, we measured several gene expressions in mouse intestinal segments for each experiment. Most of the variability observed in gene expression was due to the intestinal segment (**Figure 2P**). Although no difference in specific intestinal segment was observed, *Scar1b* and *Abca1* were globally significantly downregulated and upregulated, respectively, in the AI-3d-treated group receiving γ-tocopherol compared to the control group ($p < 0.05$; **Figure 2P; Left panel**). The proteins SR-BI and ABCA1 encoded by these two genes have been implicated in vitamin E uptake[4] and apo-AI-mediated HDL basolateral efflux[36] in mouse enterocytes, respectively. This could participate in lowering the effect of AI-3d treatment on tocopherol absorption. At dietary dose of cholecalciferol, AI-3d treatment also induced modifications in the expression of genes implicated in fat-soluble vitamin and lipid intestinal metabolism (**Figure 2P; Right panel**). Meanwhile, at high cholecalciferol dose, no impact of AI-3d treatment on gene expression was observed (**Figure S1M**).

Cooperation between membrane transporters and Aster proteins for vitamins E and D transport through Caco-2 TC7 intestinal cells

Given the importance of NPC1L1 to load cholesterol at the enterocyte plasma membrane prior to Aster proteins action[15,16], and because NPC1L1 have previously been involved in the absorption of both vitamin E[37–39] and D[5], we explored the potential complementary roles of these proteins regarding vitamins E and D transport.

Differentiated Caco-2 TC7 were incubated with vitamin-loaded micelles (with or without cholesterol) and ezetimibe, a well know chemical inhibitor of NPC1L1[40], +/- AI-3d. As expected, NPC1L1 inhibition by ezetimibe induced a marked reduction of basolateral secretion of both α-tocopherol and cholecalciferol independently of the presence of micellar cholesterol. This reduction was greater than that induced by AI-3d alone and was not further increased when both proteins were inhibited (**Figures 3A and 3B**). These results suggest that the transport of vitamins E and D relies on an NPC1L1-mediated process. Aster protein-mediated transfer of vitamin is likely engaged downstream NPC1L1 uptake because no further inhibition of secretion was observed with AI-3d treatment.

We also explored the putative cooperation of Aster proteins with SR-BI, considering their closely related functions in the adrenal gland[15] and the association between this protein and vitamins E and D uptakes[4–6]. SR-BI is not essential for cholesterol absorption but serves as a lipid sensor[41]. After micelle exposure, it relocates to raft-lipid domain and activates downstream pathways that initiate chylomicron synthesis[41–43]. In Caco-2 TC7, SR-BI inhibitor BLT1[4] alone did not impact substantially cholecalciferol secretion (**Figure 3B**). Again the incubation time and micellar concentration used here likely explain the contrasting results previously obtained in the same model[44]. Interestingly, BLT1 treatment along with AI-3d induced an additional reduction of both vitamin secretion (**Figures 3A and 3B**).

As AI-3d effect was more pronounced with α-tocopherol, we aimed to confirm the potential implication of SR-BI along Aster proteins in α-tocopherol transport by using two *SCARB1*-KO Caco2 TC7 clones (named C3.6 and D4.4) developed with the CRISPR-Cas9 methodology (see **Figure S2** for the full characterization

of the clones). α-tocopherol basolateral secretion by C3.6 *SCARB1*-KO clone was not affected by AI-3d treatment but a significant diminution was observed for D4.4 clone, although remaining non-significant (**Figure 3C**). This lack of effect of AI-3d is likely due to differences in gene expression between the clones and the native cells. There was notably a diminution of *GRAMD1B* expression and an upregulation of *APOB48* and *ABCA1* that would increase chylomicron or HDL secretion in the clones, both regulations being more pronounced in the C3.6 clone (**Figure S2G**). These results suggest that the transport of vitamins E and D also relies on an SR-BI-mediated process. The additional effect of AI-3d compared to BLT1 indicates that the SR-BI protein may also act independently on vitamin absorption, in addition to cooperating with the Asters proteins.

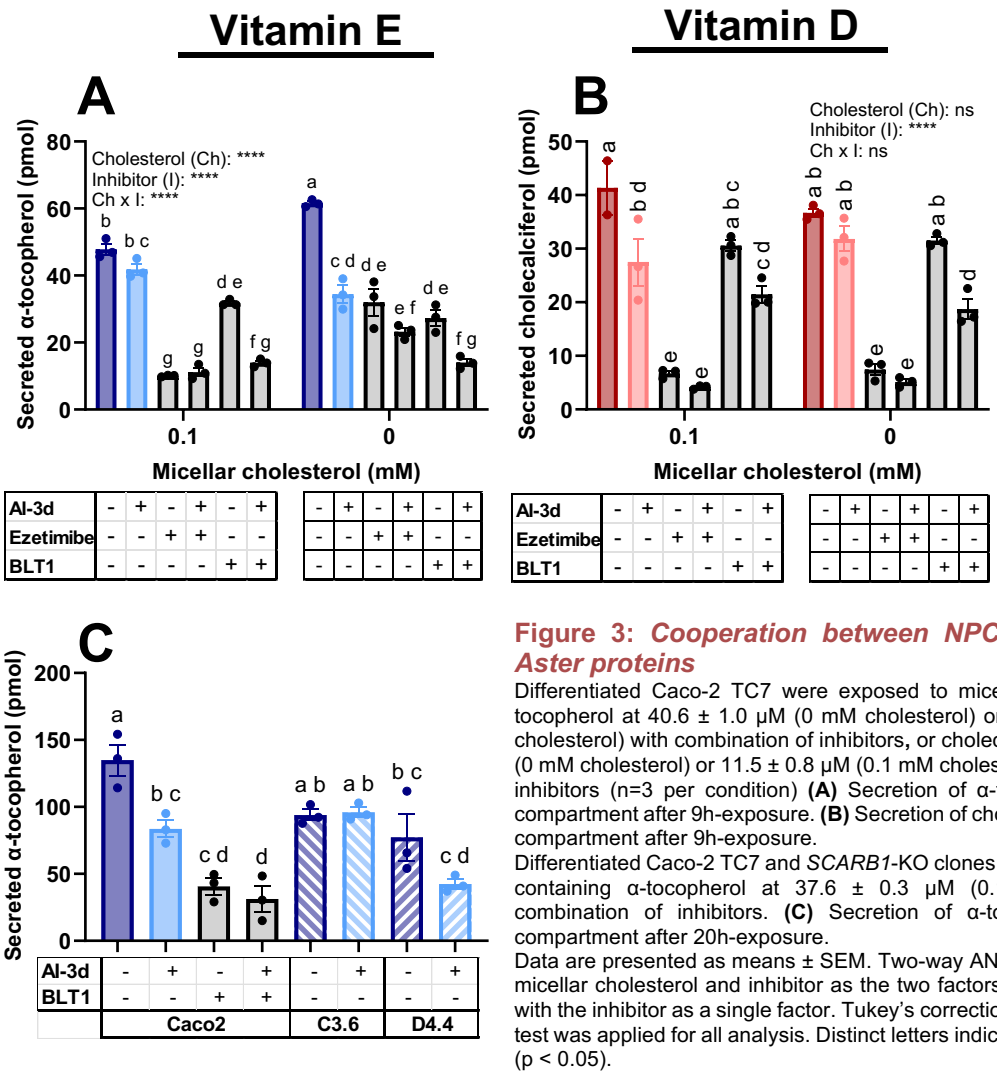


Figure 3: ***Cooperation between NPC1L1 or SR-BI and Aster proteins***

Differentiated Caco-2 TC7 were exposed to micelles containing either α-tocopherol at 40.6 ± 1.0 µM (0 mM cholesterol) or 42.3 ± 1.1 µM (0.1 mM cholesterol) with combination of inhibitors**,** or cholecalciferol at 10.0 ± 0.2 µM (0 mM cholesterol) or 11.5 ± 0.8 µM (0.1 mM cholesterol) with combination of inhibitors (n=3 per condition) **(A)** Secretion of α-tocopherol in basolateral compartment after 9h-exposure. **(B)** Secretion of cholecalciferol in basolateral compartment after 9h-exposure.

Differentiated Caco-2 TC7 and *SCARB1*-KO clones were exposed to micelles containing α-tocopherol at 37.6 ± 0.3 µM (0.1 mM cholesterol) with combination of inhibitors. **(C)** Secretion of α-tocopherol in basolateral compartment after 20h-exposure.

Data are presented as means ± SEM. Two-way ANOVA for A and B with the micellar cholesterol and inhibitor as the two factors. One-way ANOVA for C with the inhibitor as a single factor. Tukey's correction for multiple comparison test was applied for all analysis. Distinct letters indicate significant differences ($p < 0.05$).

Involvement of endocytosis in vitamins A, E and D trafficking in the enterocyte

An alternative, or complementary, mechanism to non-vesicular Aster-mediated pathway could be an endocytic process[12,14]. To test this hypothesis, we applied pharmacological inhibitors targeting assembly or movement of endocytic vesicles in our Caco-2 TC7 model. The incubation times of the different inhibitors were chosen depending on the results obtained for retinol esterification (**Figure 1C**) or regarding secretion kinetics (**Figures 4D and 4J**).

Thus, after 20h incubation, chlorpromazine, which prevent AP2 assembly necessary for clathrin-coat pit formation [45], modified retinol uptake and esterification (**Figure 4A**). Conversely, chlorpromazine, did not

impact α-tocopherol uptake (**Figures 4C and 4E**) but significantly decreased its secretion (**Figures 4D and 4F**). In the case of cholecalciferol, chlorpromazine induced a slight increase in uptake after 20h incubation (**Figure 4I and 4K**) and a significant decrease in its basolateral secretion (**Figures 4J and 4N**).

Lipid raft/caveolae-mediated endocytosis disturbance by MβCD cholesterol depletion[45] moderately but significantly decreased vitamin A uptake (**Figure 4B)**. Tocopherol uptake was also significantly decreased by MβCD (**Figures 4C and 4G**) but not its secretion (**Figures 4D and 4H**). Regarding cholecalciferol, treatment with MβCD induced both a diminution of uptake and secretion after 9h incubation (**Figures 4M and 4N**), although after 24h, uptake levels were comparable (**Figures 4I and 4J**).

Overall, these results suggest the involvement of endocytosis in vitamin E and D intracellular transport. However, it is difficult to really dissociate this pathway from a transporter-mediated absorption route. Indeed, multiple studies have observed clathrin-mediated NPC1L1 endocytosis after lipid and/or cholesterol loading[22,40,46,47]. Similarly, the effect of MβCD on vitamin absorption can support the role of lipid-raft in SR-BI-mediated uptake [48].

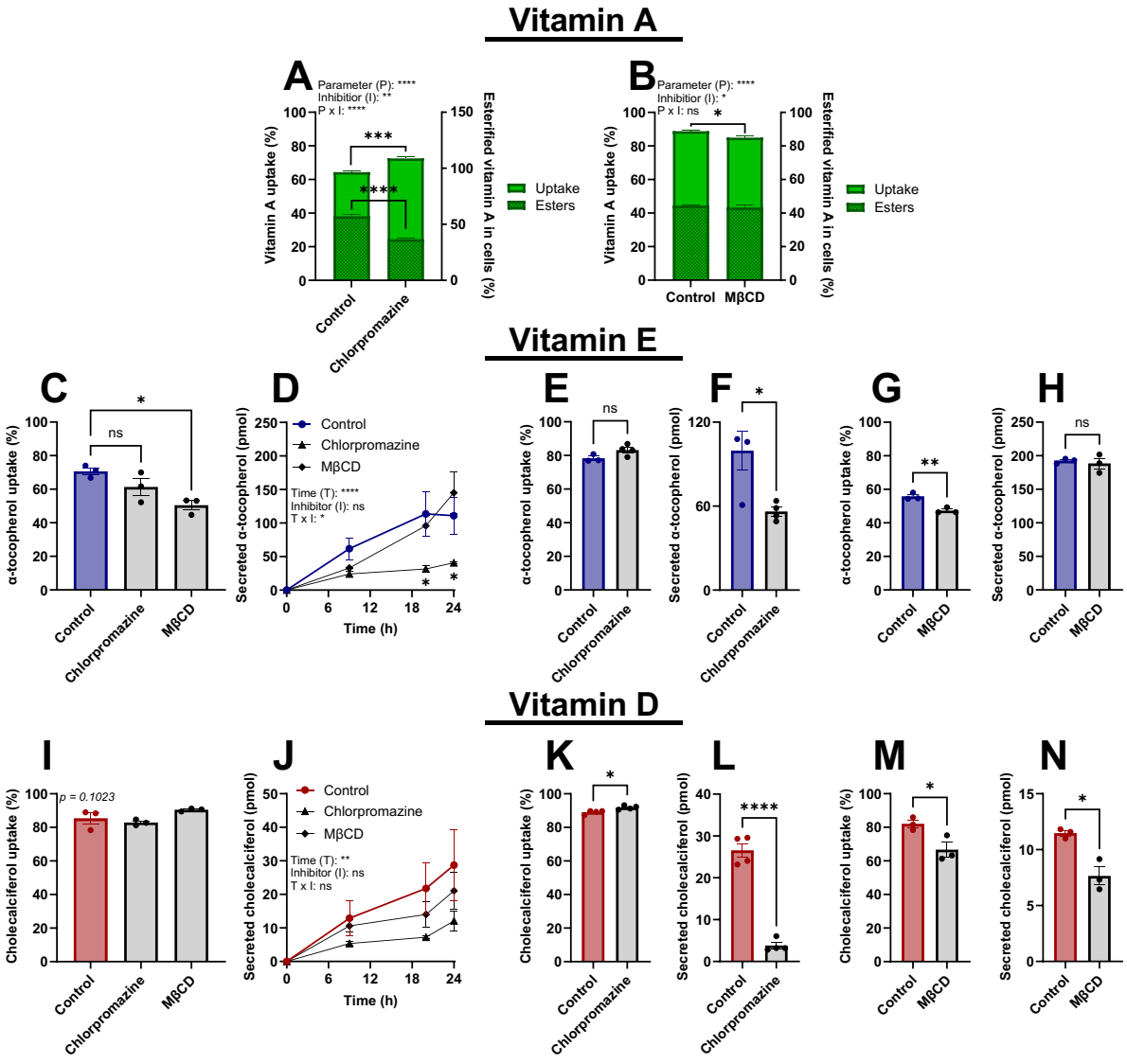


Figure 4: ***Complementary involvement of endocytosis in vitamin A, E and D traffic through the enterocyte***

Differentiated Caco-2 TC7 were exposed to micelles containing retinol (7.7 ± 0.0 µM to 9.6 ± n.m µM) and supplemented with either DMSO (control) or an endocytosis inhibitor (n=4 per condition, 20h incubation), Uptake and esterified vitamin A in cells in the presence or not of 50 µM Chlorpromazine **(A)** or in the presence or not of 10 mM MβCD **(B).**

Differentiated Caco-2 TC7 were exposed to micelles containing α-tocopherol (58.7 ± 0.5 µM) with either DMSO, Chlorpromazine or MβCD (n=3 per condition, up to 24h incubation)**, (C)** Uptake of α-tocopherol, **(D)** Secretion of α-tocopherol in basolateral compartment depending on the incubation time.

Differentiated Caco-2 TC7 were exposed to micelles containing α-tocopherol (44.0 ± 0.4 µM) with either DMSO or Chlorpromazine (n=4 per condition, 20h incubation)**.** (**E)** Uptake of α-tocopherol, **(F)** Secretion of α-tocopherol in basolateral compartment depending on the incubation time.

Differentiated Caco-2 TC7 were exposed to micelles containing α-tocopherol (37.3 ± n.m µM) with either DMSO or MβCD (n=4 per condition, 9h incubation)**; (G)** Uptake of α-tocopherol; **(H)** Secretion of α-tocopherol in basolateral compartment.

Panels **(I)** to **(N)** corresponds respectively to panels (C) to (H) with micelles containing cholecalciferol (7 µM ± n.m to 12.3 ± 0.3 µM) instead of α-tocopherol.

Data are presented as means ± SEM. Repeated-Measures Two-way ANOVA for A and B. One-way ANOVA for C and D and Geisser-Greenhouse corrected Repeated Measures Two-way ANOVA for D and J with Dunnett's correction for multiple comparison tests. Unpaired two-tailed t-test for E-H and K-N, with Welch's correction when necessary. Ns non-significant, *p < 0.05, **p < 0.01, ***p < 0.001 and ****p < 0.0001.

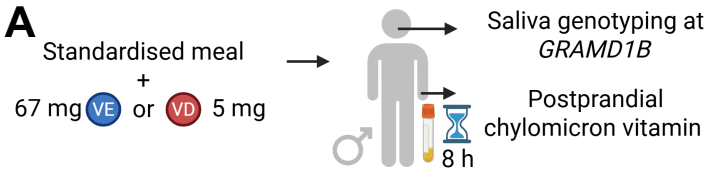
Single nucleotide polymorphisms in GRAMD1B *are associated with vitamin D bioavailability in an exploratory analysis in healthy male adults*

We finally investigated the association between genetic variability in Aster-encoding genes and the bioavailability of vitamin D and E (**Figure 5A**). Single-cell RNA-seq analysis of intestinal enterocytes indicated that *GRAMD1B* and *GRAMD1C* tend to be more highly expressed than *GRAMD1A*, consistent with previous reports[13,16]. Based on these observations, SNP analyses were restricted to *GRAMD1B* and *GRAMD1C*.

For vitamin E, no single nucleotide polymorphism (SNP) showed a significant association after correction for multiple testing under any of the adjustment models, suggesting that common genetic variation in these genes does not play a major role in interindividual variability in vitamin E bioavailability in this cohort.

In contrast, several SNPs in *GRAMD1B* were associated with vitamin D bioavailability, although these associations depended on the adjustment strategy. In unadjusted and partially adjusted models (age, BMI, and fasting triglycerides), no significant associations were observed (minimum adjusted *p*-values of 0.217 and 0.143, respectively). Significant associations emerged in the primary model (model 3), which included adjustment for metabolic covariates, including age, BMI, fasting triglycerides, cholesterol, and fasting vitamin D concentrations. In this model, five SNPs within *GRAMD1B* reached statistical significance after correction for multiple testing, namely rs12291891, rs2078158, rs1274214, rs732211, and rs1148093 (adjusted *p*-values ranging from 0.035 to 0.042). The characteristics of these SNPs are summarized in **(Figure 5B)**. Linkage disequilibrium (LD) analysis indicated that these variants were not in strong LD (maximum R^2 = 0.677), suggesting that they do not represent a single association signal and may reflect multiple independent or partially correlated variants. No previously reported associations were identified for these SNPs or their proxies (R^2 > 0.8) using the LDlink platform, suggesting that these variants have not been previously linked to known phenotypes. All five SNPs were intronic variants with relatively high minor allele frequencies, suggesting that the observed associations may be driven by regulatory mechanisms rather than protein-coding changes. Functional annotation using RegulomeDB and FORGEdb further supported this interpretation, as several of the identified SNPs showed strong regulatory potential. In particular, rs1274214 and rs732211 showed strong evidence of regulatory activity (RegulomeDB rank 1f; FORGEdb scores 7 and 8, respectively), while rs1148093 also displayed substantial regulatory evidence (rank 2b; FORGEdb score 6). Although no expression quantitative trait loci (eQTLs) were identified in the GTEx database, this does not preclude a regulatory role for these variants, as GTEx may lack sensitivity for detecting context-specific or cell-type-specific effects, particularly in intestinal epithelial cells and postprandial conditions.

The fact that all significant variants map to *GRAMD1B* further supports a potential role of this gene in vitamin D bioavailability. The emergence of associations only after adjustment for metabolic variables suggests that interindividual variability in lipid status and baseline vitamin D levels may mask underlying genetic effects in simpler models. Controlling for these factors may therefore enhance the detection of genetic contributions to vitamin D bioavailability.



B

SNP	Gene	Location	MAF[a]	BH-adjusted p			Regulome DB[c]	FORGEdb score[d]
				Unadjusted[b]	model 2[b]	model 3[b]		
rs12291891	*GRAMD1B*	intronic	T=0.34	0.217	0.143	0.035	4	5
rs2078158	*GRAMD1B*	intronic	A=0.34	0.281	0.143	0.035	5	5
rs1274214	*GRAMD1B*	intronic	C=0.49	0.550	0.215	0.035	1f	7
rs732211	*GRAMD1B*	intronic	C=0.40	0.281	0.215	0.035	1f	8
rs1148093	*GRAMD1B*	intronic	G=0.47	0.217	0.143	0.042	2b	6

Figure 5: *Association of SNPs with bioavailability of vitamin D*

(A) Clinical trial study design. **(B)** Characteristics of SNPs in GRAMD1B significantly associated with vitamin D bioavailability after adjustment for metabolic covariates (model 3). [a]Alternate allele frequencies were retrieved from dbSNP (https://www.ncbi.nlm.nih.gov/snp/) using the Allele Frequency Aggregator (ALFA) dataset (pooled allele frequency data from dbSNP and the dbGaP) in the global population (24.04.2026). MAF: minor allele frequency. [b]Values correspond to Benjamini–Hochberg-adjusted p-values. Model 2 was adjusted for age, BMI, and fasting TG; model 3 was adjusted for age, BMI, fasting TG, fasting cholesterol, and fasting vitamin D concentration. Model 3 was considered the primary model. BH: Benjamini–Hochberg. [c]RegulomeDB scores range from 1 to 7, with lower scores indicating stronger evidence of regulatory function. Letter annotations (a–f) further specify the type and strength of supporting evidence. [d]FORGEdb score integrates multiple lines of functional genomic evidence, with higher scores indicating stronger support for regulatory activity.

LIMITS OF THE STUDY

The authors acknowledge that several limitations can be identified in our study. Firstly, most of our results rely on the use of pharmacological inhibitors that can display unspecific actions to the protein/process they are targeting[49]. However, this approach can help identify drugs that could be later used in clinical treatment, as for ezetimibe for example. Also, this approach can prevent adaptative regulations of cell gene expression as it was observed in our *SCARB1*-KO clones. Secondly, Caco-2 TC7 model does not represent all the physiological features of the intestine and has a low capacity of secretion[28], which explain in part the long incubation times applied here to allow satisfying quantification of vitamin secretion. The mouse model provides all physiological parameters that the Caco-2 model does not offer. However, it brings also limitations inherent to laboratory animal models[50]. Especially in the case of mice, it seems that gastric emptying[50] as well as expression of some intestinal proteins differ[51]. Regarding genetic association analysis, it should be noted that there was a strong dependence of the results on the adjustment strategy and a limited sample size. Therefore, these findings should be considered exploratory. Further studies in larger cohorts will be required to confirm these associations and clarify the underlying mechanisms.

CONCLUSION

Overall, this work shows for the first time that Aster proteins, which participate in intracellular transfer of cholesterol and xanthophylls from the plasma membrane to endoplasmic reticulum where it is esterified[16,18], also participate in vitamin E and D intracellular transport downstream to their membrane transporters in enterocytes. The fact that only secreted amount of cholecalciferol and α-tocopherol, and not vitamin uptake, were decreased in a Caco-2 TC7 model treated with AI-3d comforted the hypothesis that Aster proteins would be implicated in the intracellular transport but not in the apical membrane uptake of these two vitamins. On the other hand, retinol esterification remained unaffected by the treatment, which further underlines the major role of specific proteins to target retinol to the ER[9]. Interestingly, we observed that AI-3d reduced α-tocopherol and cholecalciferol secretions even in absence of micellar cholesterol, suggesting that micellar components, including α-tocopherol and cholecalciferol, are likely able to induce the binding of Aster proteins to the plasma membrane even when no accessible cholesterol is added to the membrane[15]. An endocytosis process has been suggested to partly mediate vitamin absorption, though these observations need further validation. Importantly, our genetic association analysis in a human intervention study suggests that variants in *GRAMD1B* may contribute to interindividual variability in vitamin D bioavailability, supporting the physiological relevance of Aster-mediated pathways (See **Figure 6** for summary).

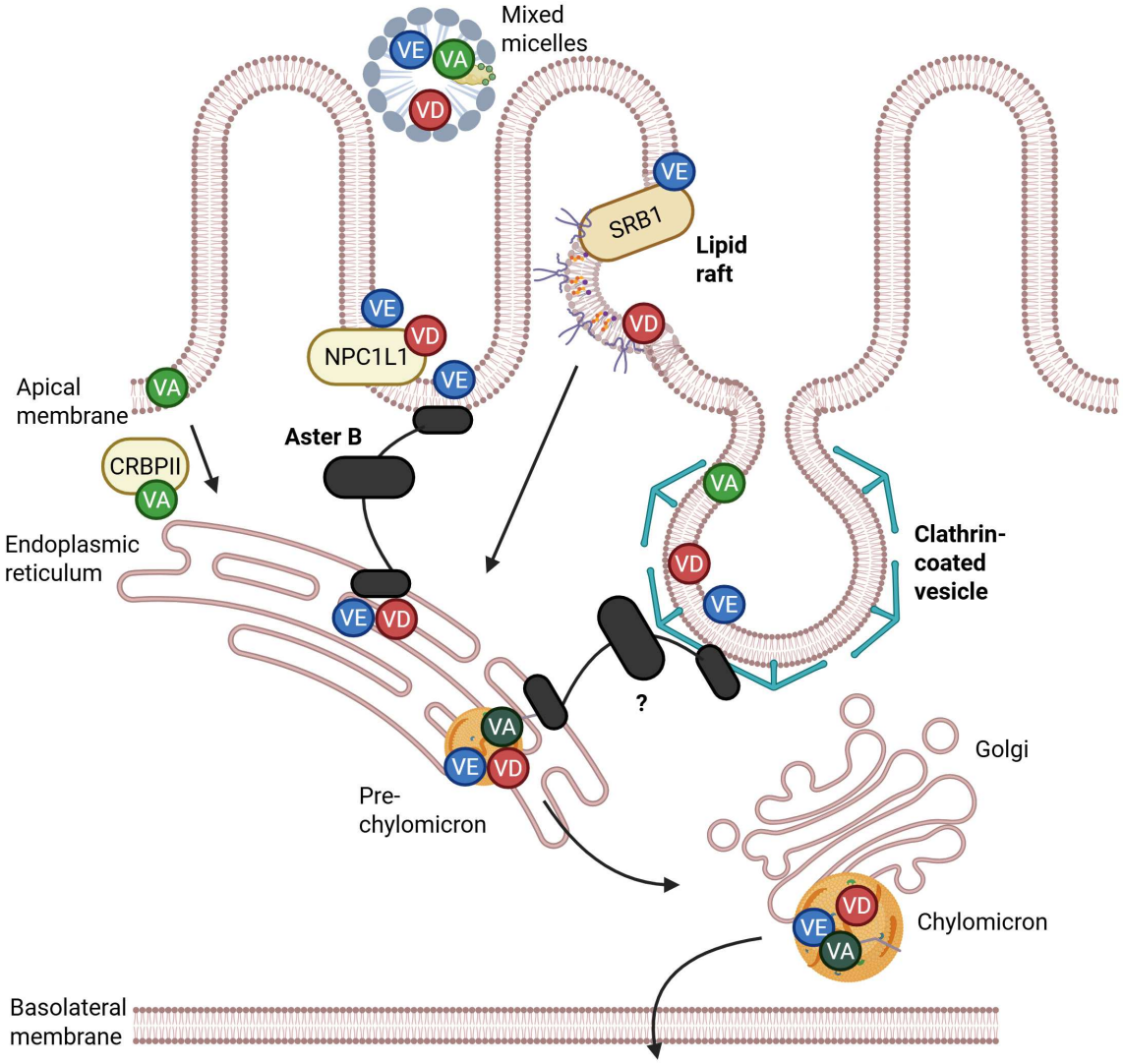


Figure 6: ***Fat-soluble vitamin intracellular trafficking within the enterocyte***

VA: vitamin A (retinol), VD: vitamin D (cholescalciferol), VE: vitamin E (tocopherol).

Vitamins D and E are taken up from mixed micelles by the apical membrane transporters SR-BI (Scavenger Receptor class B type I) and/or NPC1L1 (Niemann-Pick C1-Like 1). The mechanism by which vitamin A crosses the apical membrane remains unknown. Aster proteins are involved in the intracellular transport of vitamin D and E to the endoplasmic reticulum, while CRBPII supports retinol trafficking. An endocytotic process may be involved in the 3 vitamin routing process to the reticulum, in association or not with Aster proteins. Only vitamin A is re-esterified before secretion into chylomicrons. Pre-chylomicrons are then exported to the Golgi apparatus where they mature into chylomicrons before being released to the lymphatic system.

RESOURCE AVAILABILITY

Lead contact

Requests for further information and resources should be directed to and will be fulfilled by the lead contact, Emmanuelle Reboul (Emmanuelle.Reboul@inrae.fr).

Materials availability

All unique/stable reagents generated in this study are available from the lead contact with a completed materials transfer agreement.

Data and code availability

Data

All data have been deposited at Data INRAE and are publicly available as of the date of publication at https://doi.org/10.57745/KTR0A4.

Code

This paper does not report original code.

Additional information

Any additional information required to reanalyze the data reported in this paper is available from the lead contact upon request.

ACKNOWLEDGMENTS

Authors are grateful to the Centre d'Exploration Fonctionnel Scientifique Platform, for assistance in *in vivo* experiments, especially to Renan Benevides Tchalikan. Authors would like to thank Julien Astier, Teresa Gonzalez and Ella Flores (C2VN, Marseille, France) for their support in the experiments. Angélique Berthomé received a doctoral fellowship (2023-2026) from Region Provence Alpes Côte d'Azur in partnership with the Centre Technique de Conservation des Produits Alimentaires (CTCPA, Avignon, France). Marine Chotard PhD fellowship was funded by the French Government ANR grant (ANR-24-CE14-6425).

AUTHOR CONTRIBUTIONS

Conceptualization, E.R. and A.B.; methodology, E.R., D.V., C.S., C.D., P.B., and A.B.; Investigation, A.B., D.V., M.C., C.D., M.P.Z. C.S., A.B.N., C.S. and E.R.; writing—original draft, A.B., D.V., C.D. and E.R.; writing—review & editing, P.B.; funding acquisition, E.R.; resources, E.R. and P.B.; supervision, E.R.

DECLARATION OF INTERESTS

The authors declare no competing interests.

DECLARATION OF GENERATIVE AI AND AI-ASSISTED TECHNOLOGIES

Not applicable.

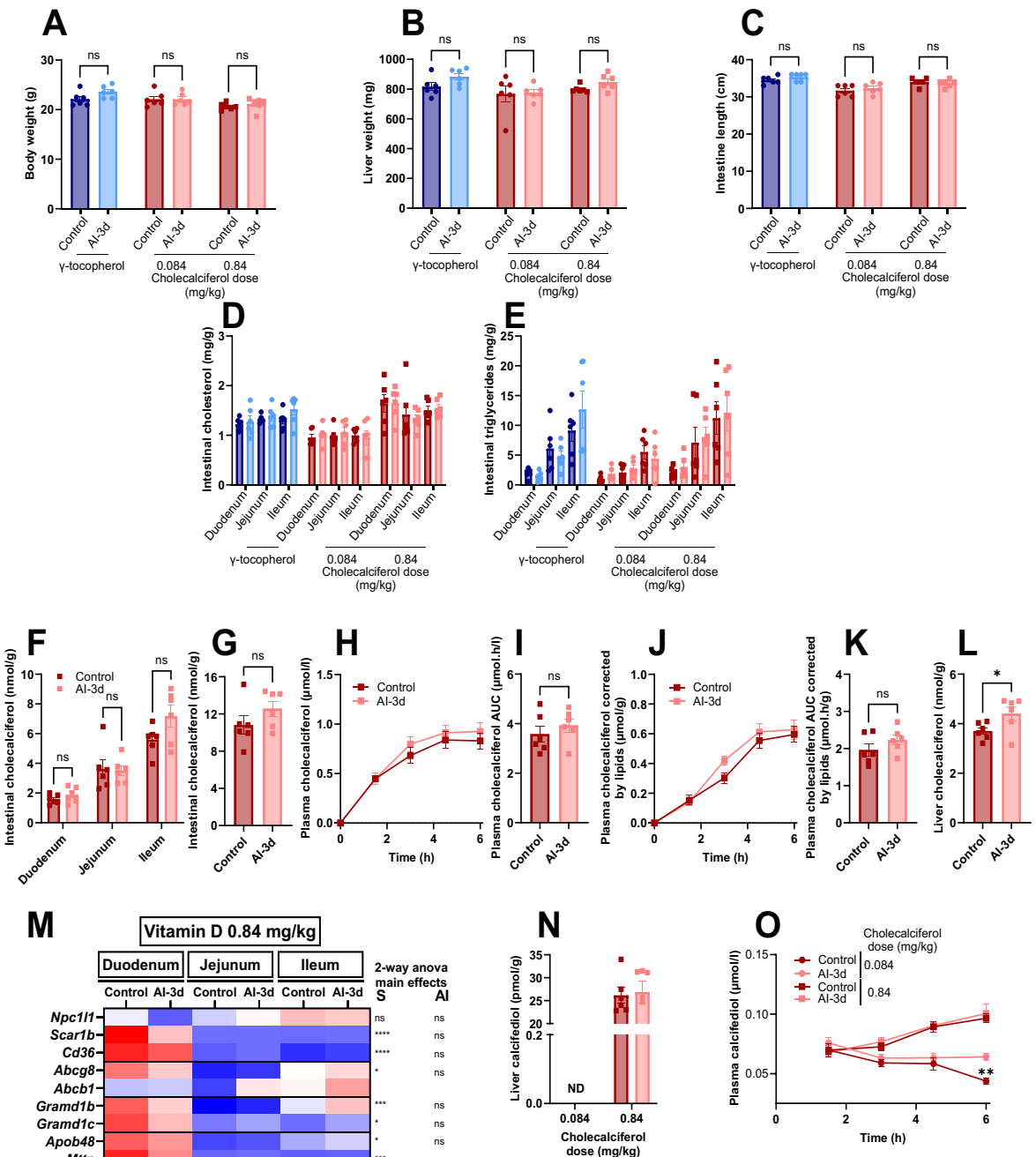


Figure *S1:* Additional measures in mice, related to Figure 2

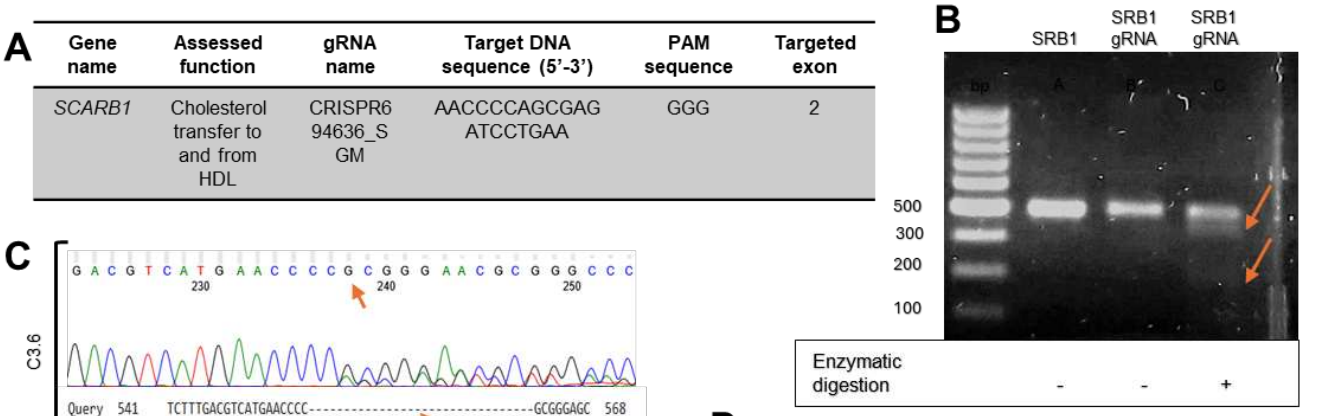
Additional measures in mice from the 3 independent experiments described in Figure 2. **(A)** Body weight. **(B)** Liver weight. **(C)** Intestinal length. **(D)** Intestinal cholesterol concentration. **(E)** Intestinal triglycerides concentration.

For mice force-fed cholecalciferol at 0.84 mg/kg: **(F)** cholecalciferol measured in intestinal segments at the end of the postprandial phase; **(G)** cholecalciferol total intestinal content.; **(H)** Plasma cholecalciferol was monitored up to 6h after force-feeding; **(I)** area under the curve of cholecalciferol postprandial plasma responses; (J) Postprandial plasma cholecalciferol responses corrected by plasma lipids (triglycerides + cholesterol), (K) Area under the curve of cholecalciferol postprandial responses after correction by lipids; (L) Hepatic cholecalciferol measured at the end of the postprandial phase; **(M)** Gene expression in intestinal segments; **(N)** Hepatic and **(O)** Plasma calcifediol concentrations in mice force-fed cholecalciferol.

Data are presented as means ± SEM. For each independent experiment: Unpaired two-tailed t-test for A, B, C, G and L and one-tailed for I and K. Geisser-Greenhouse corrected Repeated Measures Two-way ANOVA with Šidák's multiple comparison test for D, E, F, H, J, M, N and O. Ns non-significant, *p < 0.05, **p < 0.01, ***p < 0.001 and ****p < 0.0001. For panel P, are reported p-values associated with main effects Intestinal Segment (S) and Control or AI-3d Groups (AI), no significant interaction was detected for each gene in each experiment. Asterisks or values close to *p < 0.05 significance reported in the Heatmap corresponds to differences between Control and AI-3d Group in one segment.

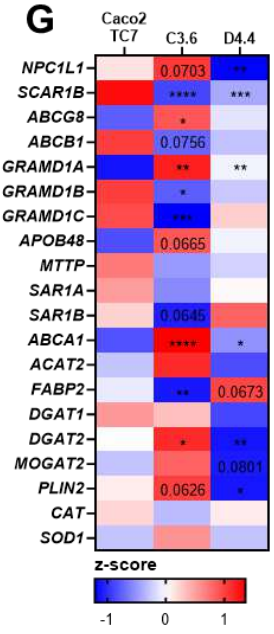
A

Gene name	Assessed function	gRNA name	Target DNA sequence (5'-3')	PAM sequence	Targeted exon
SCARB1	Cholesterol transfer to and from HDL	CRISPR6 94636_S GM	AACCCCAGCGAG ATCCTGAA	GGG	2



F

Actual genomic hit	Mismatches	Gene	Crispr Score	CFD score	ATLAS expression score	Off-targets detected
AtCCCtttCaAG ATCCTGAA-AGG	5	(EHMT1 - euchromatic histone-lysine N-methyltransferase 1)	1.281379e-08	0.172348485	33,1	C3.6: NO D4.4: NO
ttCtCCAGCaA GgTCCTGAA-GGG	5	CNTNAP2 - contactin associated protein-like 2	1.755243e-08	0.35415020	4,9	C3.6: NO D4.4: NO
tcaCCCAGtGA cATCCTGAA-GGG	5	PSMD7 - proteasome (prosome, macropain) 26S subunit, non-ATPase, 7	1.042109e-08	0.31544118	318,1	C3.6: NO D4.4: NO
AACCCCAcCc AagTCCTGAA-TGG	4	ROR1 - receptor tyrosine kinase-like orphan receptor 1	2.016921e-08	0.149832776	20,5	C3.6: NO D4.4: NO
AAaCCCAGCa AGgcCCTGAA-AGG	4	HDHD1 - haloacid dehalogenase-like hydrolase domain containing 1	1.157842e-07	0.150724638	56,7	C3.6: NO D4.4: NO



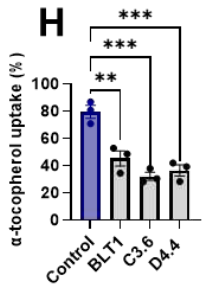


Figure *S2 Validation of SR-BI-KO Caco-2 C3.6 and D4.4, related to Figure 3*

Several clones were produced and two, named C3.6 and D4.4 were kept. (A) DNA sequence targeted by guide-RNA used in CRISPRCas9 experiment. (B) Assessment of SR-BI gRNA efficiency in Caco-2 TC7. (C) Example of the targeted region in the SCAR1B gene. (D) Quantitative analysis of SR-BI gene expression in SR-BI-mutated Caco-2/TC7 clones. (E) SR-BI protein expression in SR-BI-mutated Caco-2 TC7 clones. (F) Off-target analysis of SR-BI-mutated Caco-2 TC7 clones. (G) Z-score of gene expression (n=4 per condition), with Brown-Forsythe and Welch ANOVA with Dunnett's multiple comparison test for each gene. *p < 0.05, **p < 0.01, ***p < 0.001 and ****p < 0.0001 compared to Caco-2 TC7. (H) Secreted α-tocopherol by differentiated Caco-2 TC7 and *SCARB1*-KO exposed 20 h to micelles containing α-tocopherol at 37.6 ± 0.3 µM (0.1 mM cholesterol), One-way ANOVA with Dunnett's multiple comparison test compared to Control, **p < 0.01, ***p < 0.001.

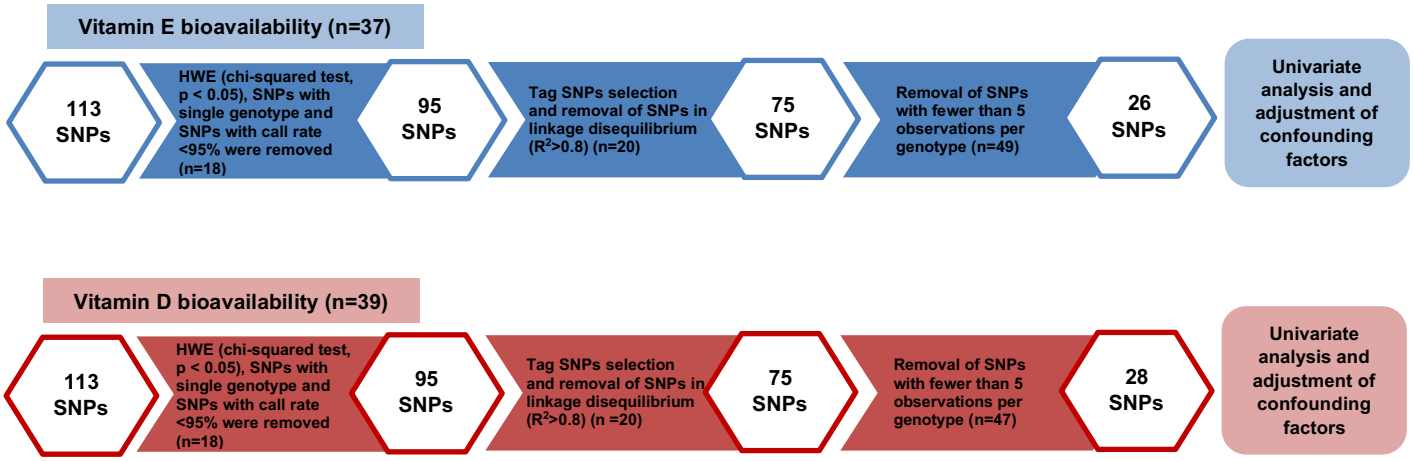


Figure S3 SNP selection flowchart (Vitamin E and vitamin D bioavailability).

381
382

REFERENCES

1. Widdowson, E.M. (1992). The Contribution of Nutrition to Human and Animal Health (Cambridge University Press).
2. Yao, M., Xiao, H., and McClements, D.J. (2014). Delivery of Lipophilic Bioactives: Assembly, Disassembly, and Reassembly of Lipid Nanoparticles. Annual Review of Food Science and Technology *5*, 53–81. https://doi.org/10.1146/annurev-food-072913-100350.
3. Goncalves, A., Roi, S., Nowicki, M., Dhaussy, A., Huertas, A., Amiot, M.-J., and Reboul, E. (2015). Fat-soluble vitamin intestinal absorption: Absorption sites in the intestine and interactions for absorption. Food Chemistry *172*, 155–160. https://doi.org/10.1016/j.foodchem.2014.09.021.
4. Reboul, E., Klein, A., Bietrix, F., Gleize, B., Malezet-Desmoulins, C., Schneider, M., Margotat, A., Lagrost, L., Collet, X., and Borel, P. (2006). Scavenger Receptor Class B Type I (SR-BI) Is Involved in Vitamin E Transport across the Enterocyte *. Journal of Biological Chemistry *281*, 4739–4745. https://doi.org/10.1074/jbc.M509042200.
5. Reboul, E., Goncalves, A., Comera, C., Bott, R., Nowicki, M., Landrier, J.-F., Jourdheuil-Rahmani, D., DUFOUR, C., Collet, X., and Borel, P. (2011). Vitamin D intestinal absorption is not a simple passive diffusion: Evidences for involvement of cholesterol transporters. Molecular nutrition & food research *55*, 691–702. https://doi.org/10.1002/mnfr.201000553.
6. Kiourtzidis, M., Kühn, J., Brandsch, C., and Stangl, G.I. (2020). Vitamin D Status of Mice Deficient in Scavenger Receptor Class B Type 1, Cluster Determinant 36 and ATP-Binding Cassette Proteins G5/G8. Nutrients *12*, 2169. https://doi.org/10.3390/nu12082169.
7. Borel, P., Lietz, G., Goncalves, A., Szabo de Edelenyi, F., Lecompte, S., Curtis, P., Goumidi, L., Caslake, M.J., Miles, E.A., Packard, C., et al. (2013). CD36 and SR-BI Are Involved in Cellular Uptake of Provitamin A Carotenoids by Caco-2 and HEK Cells, and Some of Their Genetic Variants Are Associated with Plasma Concentrations of These Micronutrients in Humans. The Journal of Nutrition *143*, 448–456. https://doi.org/10.3945/jn.112.172734.
8. Borel, P., Le, H.D., and Sabatier, M. (2026). State-of-the-art on absorption mechanisms and factors affecting the bioavailability of preformed vitamin A. Prog Lipid Res *101*, 101382. https://doi.org/10.1016/j.plipres.2026.101382.
9. Wongsiriroj, N., Piantedosi, R., Palczewski, K., Goldberg, I.J., Johnston, T.P., Li, E., and Blaner, W.S. (2008). The Molecular Basis of Retinoid Absorption: A Genetic Dissection *. Journal of Biological Chemistry *283*, 13510–13519. https://doi.org/10.1074/jbc.M800777200.
10. Reboul, E. (2023). Proteins involved in fat-soluble vitamin and carotenoid transport across the intestinal cells: New insights from the past decade. Progress in Lipid Research *89*, 101208. https://doi.org/10.1016/j.plipres.2022.101208.
11. Lev, S. (2010). Non-vesicular lipid transport by lipid-transfer proteins and beyond. Nat Rev Mol Cell Biol *11*, 739–750. https://doi.org/10.1038/nrm2971.
12. Ferrari, A., and Tontonoz, P. (2025). Nonvesicular cholesterol transport in physiology. J Clin Invest *135*. https://doi.org/10.1172/JCI188127.
13. Bandara, S., Ramkumar, S., Imanishi, S., Thomas, L.D., Sawant, O.B., Imanishi, Y., and von Lintig, J. (2022). Aster proteins mediate carotenoid transport in mammalian cells. Proceedings of the National Academy of Sciences *119*, e2200068119. https://doi.org/10.1073/pnas.2200068119.
14. Reboul, E., and Borel, P. (2011). Proteins involved in uptake, intracellular transport and basolateral secretion of fat-soluble vitamins and carotenoids by mammalian enterocytes. Progress in Lipid Research *50*, 388–402. https://doi.org/10.1016/j.plipres.2011.07.001.
15. Sandhu, J., Li, S., Fairall, L., Pfisterer, S.G., Gurnett, J.E., Xiao, X., Weston, T.A., Vashi, D., Ferrari, A., Orozco, J.L., et al. (2018). Aster Proteins Facilitate Nonvesicular Plasma Membrane to ER Cholesterol Transport in Mammalian Cells. Cell *175*, 514-529.e20. https://doi.org/10.1016/j.cell.2018.08.033.
16. Ferrari, A., Whang, E., Xiao, X., Kennelly, J.P., Romartinez-Alonso, B., Mack, J.J., Weston, T., Chen, K., Kim, Y., Tol, M.J., et al. (2023). Aster-dependent nonvesicular transport facilitates dietary cholesterol uptake. Science *382*, eadf0966. https://doi.org/10.1126/science.adf0966.
17. Bandara, S., Moon, J., Ramkumar, S., and Lintig, J. von (2023). ASTER-B regulates mitochondrial carotenoid transport and homeostasis. Journal of Lipid Research *64*. https://doi.org/10.1016/j.jlr.2023.100369.

18. Bandara, S., Saadane, A., Shen, T., Yakovleva, D., Banerjee, R., Zhang, Y., Brown, J.M., and von Lintig, J. (2025). Distinct pathways for the absorption and metabolism of β-carotene and zeaxanthin in the mouse intestine. Journal of Lipid Research *66*, 100758. https://doi.org/10.1016/j.jlr.2025.100758.
19. Hansen, G.H., Niels-Christiansen, L.-L., Immerdal, L., and Danielsen, E.M. (2003). Scavenger receptor class B type I (SR-BI) in pig enterocytes: trafficking from the brush border to lipid droplets during fat absorption. Gut *52*, 1424–1431. https://doi.org/10.1136/gut.52.10.1424.
20. Hansen, G.H., Niels-Christiansen, L.-L., Immerdal, L., Nystrøm, B.T., and Danielsen, E.M. (2007). Intestinal alkaline phosphatase: selective endocytosis from the enterocyte brush border during fat absorption. American Journal of Physiology-Gastrointestinal and Liver Physiology *293*, G1325–G1332. https://doi.org/10.1152/ajpgi.00379.2007.
21. Li, P.-S., Fu, Z.-Y., Zhang, Y.-Y., Zhang, J.-H., Xu, C.-Q., Ma, Y.-T., Li, B.-L., and Song, B.-L. (2014). The clathrin adaptor Numb regulates intestinal cholesterol absorption through dynamic interaction with NPC1L1. Nat Med *20*, 80–86. https://doi.org/10.1038/nm.3417.
22. Wu, X., Ma, X.-H., Lin, J., Yang, X., Shi, J.-H., Xie, Z., Chen, Y.-X., and Zhang, W.J. (2023). Fluorescent visualization and evaluation of NPC1L1-mediated vesicular endocytosis during intestinal cholesterol absorption in mice. Life Metabolism *2*, load011. https://doi.org/10.1093/lifemeta/load011.
23. Wang, L.-J., and Song, B.-L. (2012). Niemann–Pick C1-Like 1 and cholesterol uptake. Biochimica et Biophysica Acta (BBA) - Molecular and Cell Biology of Lipids *1821*, 964–972. https://doi.org/10.1016/j.bbalip.2012.03.004.
24. Betters, J.L., and Yu, L. (2010). NPC1L1 and cholesterol transport. FEBS Letters *584*, 2740–2747. https://doi.org/10.1016/j.febslet.2010.03.030.
25. Michael Danielsen, E., and Hansen, G.H. (2006). Lipid raft organization and function in brush borders of epithelial cells (Review). Molecular Membrane Biology *23*, 71–79. https://doi.org/10.1080/09687860500445604.
26. Morel, E., Ghezzal, S., Lucchi, G., Truntzer, C., Pais de Barros, J.-P., Simon-Plas, F., Demignot, S., Mineo, C., Shaul, P.W., Leturque, A., et al. (2018). Cholesterol trafficking and raft-like membrane domain composition mediate scavenger receptor class B type 1-dependent lipid sensing in intestinal epithelial cells. Biochimica et Biophysica Acta (BBA) - Molecular and Cell Biology of Lipids *1863*, 199–211. https://doi.org/10.1016/j.bbalip.2017.11.009.
27. Xiao, X., Kim, Y., Romartinez-Alonso, B., Sirvydis, K., Ory, D.S., Schwabe, J.W.R., Jung, M.E., and Tontonoz, P. (2021). Selective Aster inhibitors distinguish vesicular and nonvesicular sterol transport mechanisms. Proc Natl Acad Sci U S A *118*, e2024149118. https://doi.org/10.1073/pnas.2024149118.
28. Levy, E., Mehran, M., and Seidman, E. (1995). Caco-2 cells as a model for intestinal lipoprotein synthesis and secretion. The FASEB Journal *9*, 626–635. https://doi.org/10.1096/fasebj.9.8.7768354.
29. Lu, F., Liang, Q., Abi-Mosleh, L., Das, A., De Brabander, J.K., Goldstein, J.L., and Brown, M.S. (2015). Identification of NPC1 as the target of U18666A, an inhibitor of lysosomal cholesterol export and Ebola infection. Elife *4*, e12177. https://doi.org/10.7554/eLife.12177.
30. During, A., and Harrison, E.H. (2007). Mechanisms of provitamin A (carotenoid) and vitamin A (retinol) transport into and out of intestinal Caco-2 cells. Journal of Lipid Research *48*, 2283–2294. https://doi.org/10.1194/jlr.M700263-JLR200.
31. Naito, T., Ercan, B., Krshnan, L., Triebl, A., Koh, D.H.Z., Wei, F.-Y., Tomizawa, K., Torta, F.T., Wenk, M.R., and Saheki, Y. (2019). Movement of accessible plasma membrane cholesterol by the GRAMD1 lipid transfer protein complex. eLife *8*, e51401. https://doi.org/10.7554/eLife.51401.
32. Goncalves, A., Gontero, B., Nowicki, M., Margier, M., Masset, G., Amiot, M.-J., and Reboul, E. (2015). Micellar lipid composition affects micelle interaction with class B scavenger receptor extracellular loops. Journal of Lipid Research *56*, 1123–1133. https://doi.org/10.1194/jlr.M057612.
33. Reagan-Shaw, S., Nihal, M., and Ahmad, N. (2008). Dose translation from animal to human studies revisited. The FASEB Journal *22*, 659–661. https://doi.org/10.1096/fj.07-9574LSF.
34. Bravo-Núñez, Á., Berthomé, A., Sabran, C., Vairo, D., Martin, J.-C., Alvarado-Ramos, K., Chassaing, B., Tomas, J., and Reboul, E. (2025). Substitution of polysorbates by plant-based emulsifiers: impact on vitamin D bioavailability and gut health in mice. Commun Biol *8*, 896. https://doi.org/10.1038/s42003-025-08293-4.
35. Alvarado-Ramos, K., Bravo-Núñez, Á., Vairo, D., Sabran, C., Landrier, J.-F., and Reboul, E. (2024). Overweight Leads to an Increase in Vitamin E Absorption and Status in Mice. Mol Nutr Food Res *68*, e2400509. https://doi.org/10.1002/mnfr.202400509.

36. Reboul, E., Trompier, D., Moussa, M., Klein, A., Landrier, J.-F., Chimini, G., and Borel, P. (2009). ATP-binding cassette transporter A1 is significantly involved in the intestinal absorption of *α*- and *γ*-tocopherol but not in that of retinyl palmitate in mice. The American Journal of Clinical Nutrition *89*, 177–184. https://doi.org/10.3945/ajcn.2008.26559.
37. Kamishikiryo, J., Haraguchi, M., Nakashima, S., Tasaka, Y., Narahara, H., Sugihara, N., Nakamura, T., and Morita, T. (2017). N-terminal domain of the cholesterol transporter Niemann–Pick C1-like 1 (NPC1L1) is essential for α-tocopherol transport. Biochemical and Biophysical Research Communications *486*, 476–480. https://doi.org/10.1016/j.bbrc.2017.03.065.
38. Narushima, K., Takada, T., Yamanashi, Y., and Suzuki, H. (2008). Niemann-Pick C1-Like 1 Mediates α-Tocopherol Transport. Molecular Pharmacology *74*, 42–49. https://doi.org/10.1124/mol.107.043034.
39. Reboul, E., Soayfane, Z., Goncalves, A., Cantiello, M., Bott, R., Nauze, M., Tercé, F., Collet, X., and Coméra, C. (2012). Respective contributions of intestinal Niemann-Pick C1-like 1 and scavenger receptor class B type I to cholesterol and tocopherol uptake: in vivov. in vitro studies. British Journal of Nutrition *107*, 1296–1304. https://doi.org/10.1017/S0007114511004405.
40. Huang, C.-S., Yu, X., Fordstrom, P., Choi, K., Chung, B.C., Roh, S.-H., Chiu, W., Zhou, M., Min, X., and Wang, Z. (2020). Cryo-EM structures of NPC1L1 reveal mechanisms of cholesterol transport and ezetimibe inhibition. Science Advances *6*, eabb1989. https://doi.org/10.1126/sciadv.abb1989.
41. Valacchi, G., and Pecorelli, A. (2025). Role of Scavenger Receptor B1 (SR-B1) in Improving Food Benefits for Human Health. Annual Review of Food Science and Technology *16*, 403–432. https://doi.org/10.1146/annurev-food-111523-121935.
42. Ko, C.-W., Qu, J., Black, D.D., and Tso, P. (2020). Regulation of intestinal lipid metabolism: current concepts and relevance to disease. Nat Rev Gastroenterol Hepatol *17*, 169–183. https://doi.org/10.1038/s41575-019-0250-7.
43. Béaslas, O., Cueille, C., Delers, F., Chateau, D., Chambaz, J., Rousset, M., and Carrière, V. (2009). Sensing of Dietary Lipids by Enterocytes: A New Role for SR-BI/CLA-1. PLOS ONE *4*, e4278. https://doi.org/10.1371/journal.pone.0004278.
44. Reboul, E., Goncalves, A., Comera, C., Bott, R., Nowicki, M., Landrier, J.-F., Jourdheuil-Rahmani, D., Dufour, C., Collet, X., and Borel, P. (2011). Vitamin D intestinal absorption is not a simple passive diffusion: Evidences for involvement of cholesterol transporters. Molecular Nutrition & Food Research *55*, 691–702. https://doi.org/10.1002/mnfr.201000553.
45. Ivanov, A.I. ed. (2008). Exocytosis and endocytosis (Humana Press).
46. Xiao, J., Dong, L.-W., Liu, S., Meng, F.-H., Xie, C., Lu, X.-Y., Zhang, W.J., Luo, J., and Song, B.-L. (2023). Bile acids-mediated intracellular cholesterol transport promotes intestinal cholesterol absorption and NPC1L1 recycling. Nat Commun *14*, 6469. https://doi.org/10.1038/s41467-023-42179-5.
47. Ge, L., Wang, J., Qi, W., Miao, H.-H., Cao, J., Qu, Y.-X., Li, B.-L., and Song, B.-L. (2008). The Cholesterol Absorption Inhibitor Ezetimibe Acts by Blocking the Sterol-Induced Internalization of NPC1L1. Cell Metabolism *7*, 508–519. https://doi.org/10.1016/j.cmet.2008.04.001.
48. Marques, P.E., Nyegaard, S., Collins, R.F., Troise, F., Freeman, S.A., Trimble, W.S., and Grinstein, S. (2019). Multimerization and Retention of the Scavenger Receptor SR-B1 in the Plasma Membrane. Developmental Cell *50*, 283-295.e5. https://doi.org/10.1016/j.devcel.2019.05.026.
49. Ivanov, A.I. (2008). Pharmacological Inhibition of Endocytic Pathways: Is It Specific Enough to Be Useful? In Exocytosis and Endocytosis Methods in Molecular Biology., A. I. Ivanov, ed. (Humana Press), pp. 15–33. https://doi.org/10.1007/978-1-59745-178-9_2.
50. Kararli, T.T. (1995). Comparison of the gastrointestinal anatomy, physiology, and biochemistry of humans and commonly used laboratory animals. Biopharmaceutics & Drug Disposition *16*, 351–380. https://doi.org/10.1002/bdd.2510160502.
51. Tang, V.T., Xiang, J., Chen, Z., McCormick, J., Abbineni, P.S., Chen, X.-W., Hoenerhoff, M., Emmer, B.T., Khoriaty, R., Lin, J.D., et al. (2024). Functional overlap between the mammalian Sar1a and Sar1b paralogs in vivo. Proceedings of the National Academy of Sciences *121*, e2322164121. https://doi.org/10.1073/pnas.2322164121.
52. Bordat, C., Vairo, D., Cuerq, C., Halimi, C., Peiretti, F., Penhoat, A., Vieille-Marchiset, A., Gonzalez, T., Michalski, M.-C., Nowicki, M., et al. (2023). Validation of Knock-Out Caco-2 TC7 Cells as Models of Enterocytes of Patients with Familial Genetic Hypobetalipoproteinemias. Nutrients *15*. https://doi.org/10.3390/nu15030505.

53. Desmarchelier, C., Borel, P., Goncalves, A., Kopec, R., Nowicki, M., Morange, S., Lesavre, N., Portugal, H., and Reboul, E. (2016). A Combination of Single-Nucleotide Polymorphisms Is Associated with Interindividual Variability in Cholecalciferol Bioavailability in Healthy Men. Journal of Nutrition *146*, 2421–2428. https://doi.org/10.3945/jn.116.237115.
54. Landrier, J.-F., Malezet-Desmoulins, C., Reboul, E., Marie Lorec, A., Josèphe Amiot, M., and Borel, P. (2008). Comparison of different vehicles to study the effect of tocopherols on gene expression in intestinal cells. Free Radical Research *42*, 523–530. https://doi.org/10.1080/10715760802098859.
55. Reboul, E., Abou, L., Mikail, C., Ghiringhelli, O., André, M., Portugal, H., Jourdheuil-Rahmani, D., Amiot, M.-J., Lairon, D., and Borel, P. (2005). Lutein transport by Caco-2 TC-7 cells occurs partly by a facilitated process involving the scavenger receptor class B type I (SR-BI). Biochem J *387*, 455–461. https://doi.org/10.1042/BJ20040554.
56. Turner, P.V., Brabb, T., Pekow, C., and Vasbinder, M.A. (2011). Administration of Substances to Laboratory Animals: Routes of Administration and Factors to Consider. Journal of the American Association for Laboratory Animal Science *50*, 600–613.
57. Margier, M., Collet, X., le May, C., Desmarchelier, C., André, F., Lebrun, C., Defoort, C., Bluteau, A., Borel, P., Lespine, A., et al. (2019). ABCB1 (P-glycoprotein) regulates vitamin D absorption and contributes to its transintestinal efflux. The FASEB Journal *33*, 2084–2094. https://doi.org/10.1096/fj.201800956R.
58. Borel, P., Desmarchelier, C., Nowicki, M., and Bott, R. (2015). Lycopene bioavailability is associated with a combination of genetic variants. Free Radical Biology and Medicine *83*, 238–244. https://doi.org/10.1016/j.freeradbiomed.2015.02.033.
59. Borel, P., Desmarchelier, C., Nowicki, M., and Bott, R. (2015). A Combination of Single-Nucleotide Polymorphisms Is Associated with Interindividual Variability in Dietary β-Carotene Bioavailability in Healthy Men1, 2, 3. The Journal of Nutrition *145*, 1740–1747. https://doi.org/10.3945/jn.115.212837.
60. Borel, P., Desmarchelier, C., Nowicki, M., Bott, R., Morange, S., and Lesavre, N. (2014). Interindividual variability of lutein bioavailability in healthy men: characterization, genetic variants involved, and relation with fasting plasma lutein concentration12345. The American Journal of Clinical Nutrition *100*, 168–175. https://doi.org/10.3945/ajcn.114.085720.
61. Borel, P., Desmarchelier, C., Nowicki, M., Bott, R., and Tourniaire, F. (2015). Can Genetic Variability in α-Tocopherol Bioavailability Explain the Heterogeneous Response to α-Tocopherol Supplements? Antioxidants & Redox Signaling *22*, 669–678. https://doi.org/10.1089/ars.2014.6144.
62. Desmarchelier, C., Borel, P., Goncalves, A., Kopec, R., Nowicki, M., Morange, S., Lesavre, N., Portugal, H., and Reboul, E. (2016). A Combination of Single-Nucleotide Polymorphisms Is Associated with Interindividual Variability in Cholecalciferol Bioavailability in Healthy Men1234. The Journal of Nutrition *146*, 2421–2428. https://doi.org/10.3945/jn.116.237115.
63. Desmarchelier, C., Martin, J.-C., Planells, R., Gastaldi, M., Nowicki, M., Goncalves, A., Valéro, R., Lairon, D., and Borel, P. (2014). The postprandial chylomicron triacylglycerol response to dietary fat in healthy male adults is significantly explained by a combination of single nucleotide polymorphisms in genes involved in triacylglycerol metabolism. J Clin Endocrinol Metab *99*, E484-488. https://doi.org/10.1210/jc.2013-3962.

STAR★METHODS

KEY RESOURCES TABLE

REAGENT OR RESOURCE	SOURCE	IDENTIFIER
Antibodies		
Biological samples		
Chemicals, peptides, and recombinant proteins		
Retinol	Sigma-Aldrich	R7632
Retinyl Palmitate	Sigma-Aldrich	PHR1235
Cholecalciferol	Sigma-Aldrich	C9756
Ergocalciferol	Sigma-Aldrich	95220
Vitamin D3(6,19,19-d3) (cholecalciferol-d3)	Sigma-Aldrich	740284
Vitamin25OHD3d3 (calcifediol-d3)	Sigma-Aldrich	739596
DL-α-tocopherol	Sigma-Aldrich	T3251
DL-γ-tocopherol	Sigma-Aldrich	T1782
Tocol	Sigma-Aldrich	AABH9A955256
Retinyl Acetate	Sigma-Aldrich	PHR1236
DL-α-tocopherol acetate	Sigma-Aldrich	T3376
4-phenyl-1,2,4-triazoline-3,5-dione (PTAD)	Sigma-Aldrich	280992
Formic acid	Sigma-Aldrich	5.33002.0050
Cholesterol	Sigma-Aldrich	C3045
2-Oleoyl-1-palmitoyl-sn-glycero-3-phosphocholine	Sigma-Aldrich	42773
1-palmitoyl-sn-glycero-3-phosphocholine	Sigma-Aldrich	L5254
Oleic Acid	Sigma-Aldrich	01008
1-Oleoyl-rac-glycerol	Sigma-Aldrich	M7765
Taurocholic acid sodium salt hydrate	Sigma-Aldrich	T4009
U18666A	Sigma-Aldrich	U3633
20-Me-HC-Pyrrolidine (AI-3d)	MedChemExpress	HY-145001
Chlorpromazine hydrochloride	Sigma-Aldrich	C8138
Methyl-β-cyclodextrin (MβCD)	Sigma-Aldrich	C4555
Ezetimibe	Sigma-Aldrich	SML1629
BLT1	Sigma-Aldrich	SML0059
Dimethyl sulfoxide (DMSO)	Sigma-Aldrich	102552110
LightCycler 480 SY Green	Roche LifeScience	3639750
Reverse Transcriptase M-MLV	ThermoFisher	28025013
100 mM dNTP Set	Invitrogen	10297-018
Random Primers	Invitrogen	48190011
Dulbecco's Phosphate Buffered Saline (PBS)	Gibco	14190-039
Dulbecco's Modified Eagle Medium (DMEM)	Gibco	14190-094
Penicillin/Streptomycin	Gibco	41965-039
MEM NEAA (100x)	Gibco	11140-035

Fœtal Bovine Serum (FBS)	Eurobio Scientific	CVFSVF00-01
Sodium Chloride	Biochemika	71376
Phosphate Buffer Saline Tablets (PBS)	Gibco	18912-014
TRI Reagent®	Sigma-Aldrich	T9424
Olive oil	Puget	0000 1325 N/O
Hexane	Carlo Erba	447041
Chloroform	Carlo Erba	438581
Propan-2-ol	Carlo Erba	412821
Methanol (MeOH)	Carlo Erba	412383
Acetonitrile LC/MS (ACN-LCMS)	Carlo Erba	412342
Acetonitrile HPLC (ACN-HPLC)	Carlo Erba	412412000
Ethanol Absolute anhydrous (EtOH)	Carlo Erba	4146082
Dichloromethane (DCM)	Carlo Erba	41262000
Milli-Q® water	Millipore	SQ 2 series 2SQ200p
Critical commercial assays		
Triglycerides GPO method kit	Biolabo	80019
Cholesterol CHOD-PAP kit	Biolabo	80106
Deposited data		
Experimental models: Cell lines		
Caco-2 TC7	Gift from Dr. M. Rousset (U178 INSERM, Paris, France)	N/A
SCARB1-KO	This paper	N/A
Experimental models: Organisms/strains		
C57BL/6JRj mice	Janvier Labs	SC-C57J-M
Oligonucleotides		
M-Fabp2-F GTC TAG CAG ACG GAA CGG AG	Integrated DNA Technologies	N/A
M-Fabp2-R TCC TTC ATA TGT GTA GGT CTG GA	Integrated DNA Technologies	N/A
M-Sar1b-F CCC AAC GCT ACA TCC CAC TT	Integrated DNA Technologies	N/A
M-Sar1b-R CAT ACT CTT CGG GCT TGC AC	Integrated DNA Technologies	N/A
M-Gramd1b-F TTG AGA TTA CGC CCT CCA GC	Integrated DNA Technologies	N/A
M-Gramd1b-R CTT TGC TGG CTG CTG CTT TC	Integrated DNA Technologies	N/A
M-Gramd1c-F ATG TGC AGC CAA GAA GTC CA	Integrated DNA Technologies	N/A
M-Gramd1c-R TAA AGC TGA CGG CCT TGG AG	Integrated DNA Technologies	N/A
M-Acat2-F AGG CTG AGA GCT AGC AGA GA	Integrated DNA Technologies	N/A
M-Acat2-R GGC ACC ATT GAA GGA GCC TAT	Integrated DNA Technologies	N/A
M-Dgat1-F CCC ATA CCC GGG ACA AAG AC	Integrated DNA Technologies	N/A
M-Dgat1-R CAG ACG ATG GCA CCT CAG AT	Integrated DNA Technologies	N/A
M-Dgat2-F ACA CCT TCT GCA CAG ACT GC	Integrated DNA Technologies	N/A
M-Dgat2-R TGC GAT CTC CTG CCA CCT TT	Integrated DNA Technologies	N/A
M-Mogat2-F GGA TCC AGA ACC GGC TAC AG	Integrated DNA Technologies	N/A
M-Mogat2-R CGA TGG GCT TCC CCA CTA TG	Integrated DNA Technologies	N/A
M-Plin2-F GCT CTC CTG TTA GGC GTC TC	Integrated DNA Technologies	N/A
M-Plin2-R TTG GCC ACT CTC ATC ACC AC	Integrated DNA Technologies	N/A

M-Sqle-F TCT CAG AAT GGT CGT CTG CG	Integrated DNA Technologies	N/A
M-Sqle-R CCC AGA ATA AGG ACG CCT CG	Integrated DNA Technologies	N/A
M-Ldlr-F CCG GAG TTG CAG CAG AAG A	Integrated DNA Technologies	N/A
M-Ldlr-R TGC ATG TCT CTG GGG ACT CA	Integrated DNA Technologies	N/A
M-Apob48-F CTG TTC AGT GGC AGC AAC AC	Eurogentec	N/A
M-Apob48-R CAA GTT GAC CAG GAC TGC CT	Eurogentec	N/A
M-Mttp-F AAG CCC CAC TCA GGC AAT TC	Eurogentec	N/A
M-Mttp-R CGG CCA CTA GGC TCT CTT TT	Eurogentec	N/A
M-Scarb1-F CTT CAC GGG CGT CCA GAA	Eurogentec	N/A
M-Scarb1-R GCT GAG TCC GTT CCA TTT GTC	Eurogentec	N/A
M-Cd36-F TTC TTC CAG CCA ATG CCT TT	Eurogentec	N/A
M-Cd36-R TCA GTG CAG AAA CAA TGG TTG TC	Eurogentec	N/A
M-Abca1-F TTC CTC AAA GTG GCT GAA GAG	Eurogentec	N/A
M-Abca1-R TGC TGG CAA AGT ACC ATC TG	Eurogentec	N/A
M-Abcg8-F GAG CAC TGT GCC TAC GTC ATC A	Eurogentec	N/A
M-Abcg8-R CGC AGG TTT GTC AGC CAG TA	Eurogentec	N/A
M-Abcb1-F TCG AAG ATG GGC AAA AAG AG	Eurogentec	N/A
M-Abcb1-R AGC GAA ACA TCC CAA ATA CG	Eurogentec	N/A
M-Cat-F GCG ACC AGA TGA AGC AGT G	Eurogentec	N/A
M-Cat-R GTG GTC AGG ACA TCA GGT CTC	Eurogentec	N/A
M-Sod1-F CAG GAC CTC ATT TTA ATC CTC AC	Eurogentec	N/A
M-Sod1-R CCC AGG TCT CCA ACA TGC	Eurogentec	N/A
M-Srebpf2-F ACC TAG ACC TCG CCA AAG GT	Eurogentec	N/A
M-Srebpf2-R GCA CGG ATA AGC AGG TTT GT	Eurogentec	N/A
M-Hmg-CoA-F TGA TTG GAG TTG GCA CCA T	Eurogentec	N/A
M-Hmg-CoA-R TGG CCA ACA CTG ACA TGC	Eurogentec	N/A
M-LXRα-F GCA ACT CAA TGA TGC CGA GTT	Eurogentec	N/A
M-LXRα-R CGT GGG AAC ATC AGT CGG TC	Eurogentec	N/A
M-RXRα-F GCC ATC TTT GAC AGG GTG CT	Eurogentec	N/A
M-RXRα-R CTC CGT CTT GTC CAT CTG CAT	Eurogentec	N/A
M-18S-F GTG GGC CTG CGG CTT AAT	Eurogentec	N/A
M-18S-R GCC AGA GTC TCG TTC GTT ATC	Eurogentec	N/A
H-GRAMD1A-F ATC CAG ATC TGC ACG GAG AG	Integrated DNA Technologies	N/A
H-GRAMD1A-R ACT CAG CGT CTT TTC AAG CA	Integrated DNA Technologies	N/A
H-GRAMD1B-F ACA CAC GAT GAA GGA GAG GT	Integrated DNA Technologies	N/A
H-GRAMD1B-R CGA GTT GGT GAA GAG GAG GT	Integrated DNA Technologies	N/A
H-GRAMD1C-F GCA GGC TAA GAG TTT CCA CAG	Integrated DNA Technologies	N/A
H-GRAMD1C-R AGT CCT CCA AAC AAC TCC AGG	Integrated DNA Technologies	N/A
H-SCARB1-F CGG CTC GGA GAG CGA CTAC	Integrated DNA Technologies	N/A
H-SCARB1-R GGG CTT ATT CTC CAT CAT CAC C	Integrated DNA Technologies	N/A
Recombinant DNA		
Software and algorithms		
Biorender.com	Biorender	N/A
GraphPad Prism 10.6.1	GraphPad	N/A

Chromeleon 7	Thermo Fischer Scientific	N/A
RStudio 2024.04. 0-735	R	N/A
LightCycler® 480 SW 1.5.1	Roche LifeScience	N/A
Primer-BLAST	NCBI	N/A
Other		

EXPERIMENTAL MODEL AND STUDY PARTICIPANT DETAILS

Caco-2 and SCARB1-KO culture

SCARB1-KO Caco-2 cells were generated using CRISPR-Cas9 and validation was assessed as previously described[52]. Knocking-out confirmation of SCARB1 is presented in Supplemental Figure 2 (**Figure S12A-F**). Briefly, Caco-2 wild-type cells were transfected with TrueGuide™ Synthetic sgRNA (CRISPR694636_SGM – ThermoFisher Scientific) and TrueCut™ Cas9 V2 protein (Thermo Fisher Scientific) to target exon 2 of the SCARB1 gene. Following transfection, viable clones were selected, cultivated, and expanded in 6-well plates. Genomic DNA was extracted from putative clones, and the targeted region was amplified by PCR. The resulting PCR products were subjected to Sanger sequencing to Genewizz (Leipzig, Germany) to confirm editing efficiency. SCARB1 mRNA and protein expression levels were subsequently analyzed by quantitative PCR (qPCR) and Western blot, respectively. Potential off-target effects were assessed in silico using the crisprScore and CFDscore algorithms implemented in RStudio (version 2024.04.0-735). Predicted off-target loci were amplified by PCR, and the corresponding amplicons were sequenced.
Caco-2 clone TC7 and *SCARB1*-KO cells were maintained in DMEM media supplemented with 8% FBS, 1% penicillin-streptomycin and 1% non-essential amino acids (supplemented DMEM), incubated at 37 °C, 10% CO_2.

C56BL/6 mice and experimental study approval

The protocol was approved by the French Ministry of Higher Education and Research and referenced under the number APAFIS #46024-2023112013358971 v4. Thirty-six 6-week-old C57BL/6 male mice were purchased from Janvier laboratory (Le Genest, St Isle, France). Three animals were housed per cage and kept under controlled light, temperature and humidity. Free access to water and standard chow diet (R03-25 irradiated, Safe, Augy, France) were provided. The animals were kept in these conditions at least 2 weeks before the experiment.

METHOD DETAILS

In vitro vitamin uptake and secretion experiments

Mixed micelles were used as vehicles to deliver vitamin to intestinal cell monolayers[54]. They were produced by pouring an appropriate volume of retinol, α-tocopherol or cholecalciferol ethanolic stock solutions, kept protected from light, in a glass tube. To the vitamin solution were added lipid solutions (in Chloroform/Methanol; 2/1; v/v) in order to obtain 0.04 mM 2-Oleoyl-1-palmitoyl-sn-glycero-3-phosphocholine, 0.16 mM 1-palmitoyl-sn-glycero-3-phosphocholine, 0.5 mM oleic acid, 0.3 mM monoolein and unless stated 0.1 mM cholesterol[55]. The mixture was dried under nitrogen and the resulting lipidic film

was dissolved into serum-free DMEM containing 5 mM taurocholic acid sodium salt hydrate. After 1 h at room temperature with regular agitations, the solution was probe-sonicated 3 min at 60% (Branson Digital Sonifier 450, Connecticut, USA) in ice and passed through a 0.22 µm filter. The vitamin-enriched micelles were aliquoted and kept at -20 °C before use.

For each vitamin uptake and secretion experiments, Caco-2 clone TC7 or *SCARB1*-KO undifferentiated cells were seeded at 30 000 or 100 000 cells/cm² on transwell plates. Apical and basolateral media were changed daily with supplemented DMEM. Once at confluency, apical and basolateral media were changed every two days with serum-free and supplemented DMEM, respectively. After 14 days, the experiment's eve, confluent differentiated cells received serum-free DMEM on both sides.

The day of the experiment, basolateral media was changed for "fresh" serum-free DMEM. Apical compartment received serum-free DMEM supplemented with 0.1% DMSO containing either one or a combination of pharmacological inhibitors. The resulting concentration of inhibitors on the cell layer were, unless stated differently, 10 µM U1866A, 5 µM AI-3d, 10 µM BLT1, 100 µM Ezetimibe, 50 µM Chlorpromazine and 10 mM MβCD, priorly tested for cytotoxicity. Plates were incubated during 1 h at 37 °C, 10% CO_2. Then, the apical media was replaced by vitamin-loaded mixed micelles enriched with the same concentration of inhibitor, expect for MβCD which was not added to prevent complexation with the vitamin, as a precaution. The incubation time varied upon the experiment between 9 h and 20-24 h, chosen after preliminary experiments. Basolateral media samples from intermediate time points were also taken up and replaced by serum-free DMEM. At the end of the incubation time, apical and basolateral media were collected. The cell monolayer was rinsed with cold PBS, scraped into PBS. All samples were kept at -80 °C until analysis.

A-tocopherol, cholecalciferol and vitamin A uptakes (%) were estimated as the amount of vitamin (for vitamin A: retinol and retinyl esters) in the cell monolayer plus, if any, in the basolateral compartment over the amount of vitamin in the cell monolayer plus basolateral and apical compartments. The secreted vitamin was established as the amount in the basolateral compartment. For vitamin A, the esterified vitamin A in cells monolayers was established as the amount of retinyl esters in the cell monolayer over the amount of vitamin A (retinol and retinyl esters) in the cell monolayer.

Mice postprandial experiment

Emulsions were used as vehicles to deliver vitamin to mice. They were made of 1/3 olive oil containing or not AI-3d 10 mg/kg[16] and 2/3 NaCl 0.9% containing 0.07% 1-palmitoyl-sn-glycero-3-phosphocholine. Both phases were agitated 5 min at 2500 rpm and then probe-sonicated 2 min at 70% in ice. Emulsions were either empty of vitamin (for pre-inhibition treatments on day 1 and 2) or enriched with γ-tocopherol (15 mg/kg) or cholecalciferol-d3 (0.084 mg/kg) or cholecalciferol (0.84 mg/kg), on the day 3.

Eight-week-old mice were randomly assigned to Control (n=6) or AI-3d (n=6) groups for each vitamin. On day 1 and 2, prior the postprandial experiment, mice were weighed and given 10 mL/kg vitamin-free emulsion according to their group as designed by Ferrari and colleagues[16]. Animals were fasted overnight and then, on day 3, were force-fed 10 ml/kg[56] vitamin-enriched emulsion. Every 1.5 h after force-feeding, blood samples were collected in heparinized tubes by submandibular, retro-orbital and finally intracardiac punctions under isoflurane anaesthesia. They were directly centrifugated at 3 000 *g*, 10 min, 20 °C and plasma were kept. After the last blood puncture at 6 h, mice were euthanised by cervical dislocation. Intestine were harvested and rinsed with cold PBS. They were cut in 3 6-cm-long segments corresponding to duodenum, jejunum and ileum. Each segment was separated in two equal pieces, with the proximal segment kept for vitamin absorption assay and the distal ones scraped to recover mucosa for gene expression. The liver was also collected. Organ samples were weighed, snap-frozen in liquid nitrogen and kept at -80 °C before analysis.

Vitamin and lipid extraction

Vitamin A, E and D from *in vitro* samples (mixed micelles, apical, cells, basolateral) and plasma of γ-tocopherol mice groups were extracted from a volume adjusted when necessary to 500 µL with Milli-Q water. Same volume of an internal standard (Retinyl acetate, tocol/tocopherol acetate or cholecalciferol-d3) in ethanol was added. This aqueous phase was mixed with 2 mL hexane at 2500 rpm, 10 min and centrifugated 10 min, 1363 *g*, 4°C. The hexane extraction was repeated and the two upper phases were

pooled and dried under nitrogen. Dry samples were dissolved into 200 µL acetonitrile/dichloromethane/methanol (ACN/DCM/MeOH; 70/20/10) or MeOH for vitamin A and E, respectively. Vitamin D samples were submitted to a derivatization step with 4-phenyl-1,2,4-triazoline-3,5-dione (PTAD) prior to resuspension in 30 or 100 µL ACN as described previously[34].
Plasma Vitamin D (cholecalciferol-d3, cholecalciferol and calcifediol) of vitamin D mice groups were extracted from 20 to 50 µL plasma with either 20 µL calcifediol-d3 along with cholecalciferol-d3 or ergocalciferol (0.4ng/ µL ethanol) as internal standards for pharmacological or dietary dose vitamin D experiments respectively. Hepatic and intestinal γ-tocopherol and solely intestinal cholecalciferol deuterated or not were extracted from 100 mg organ by Bligh & Dyer method, according to Bravo-Núñez et al., 2025[34]. At the end of the extraction, dry extracts were resuspended in MeOH or ACN/MeOH/H2O (60/38/2) for vitamin E and D respectively. An appropriate volume was kept for vitamin quantification and another volume was dried and resuspended in propan-2-ol for lipid quantification.
Hepatic vitamin D (cholecalciferol-d3, cholecalciferol and calcifediol) were extracted from 90 mg organ, first grinded in 1 mL ACN 15 min, 30 mvt/s (Retsch MM400, Eragny sur Oise, France). To the homogenate were added 20 µL internal standard (calcifediol-d3 along with cholecalciferol-d3 or ergocalciferol), agitated 5 min, 1363 *g* and centrifugated 10 min, 1363 *g*, 4 °C. The supernatant was collected and dried under nitrogen. A derivatization with PTAD was applied on the dry extract and was resuspended in acetonitrile.

Vitamin quantification

For vitamin A, E and D (the later only for mixed micelles and intestinal segment samples) quantification, the HPLC instrumentation was either a Dionex Ultimate 3000 (ThermoFisher Scientific, Waltham, USA), or Shimadzu Prominence (Shimadzu, Marne-la-Vallée, France) systems composed of a pump (LPG-3400SD or LC-20ADSP), an autosampler (WPS-3000 TSC or SIL-20AC-HT) and an oven (TCC-30005D or CTO-20AC) modules coupled with a Diode Array (DAD-3000 or SPD-M20A) and a Fluorescence (FLD-3000) detectors. Ovens were equipped with a Zorbax Eclipe XDB-C18 column 4.6 x 250 mm, 5 µm (Agilent, Santa Clara, USA) monitored at 40 °C. For vitamin E (α- and γ-tocopherol) and mixed micelle's vitamin D separation the mobile phase was MeOH at 1.5 mL/min. For vitamin D separation from intestinal segment samples, the mobile phase was ACN/MeOH/H_2O (60/38/2) at 1.5 mL/min, while for vitamin A the phase was ACN/MeOH/MeOH (70/20/10) at 1.8 mL/min. Vitamin A, E and D were detected in UV-VIS at 325, 290 and 265 nm and α-tocopherol was also detected by fluorescence with 292 and 325 nm excitation and emission wavelengths respectively. For vitamin A, three esters were correctly identified: retinyl palmitate, oleate and linoleate. The quantifications of retinyl oleate and linoleate were made by comparing to retinyl palmitate standard with a correction by their molar extinction coefficients.
For vitamin D sample (except micelles and intestinal segments) analysis, the chromatographic separation and afterwards mass spectrometry quantification were carried out with the instrumentation and the conditions described by Bravo-Núñez and colleagues[34], following a LC-MS/MS method. The HPLC system was a Vanquish-Flex (ThermoFisher Scientific) made of a pump (VF-P20-A), an autosampler (VF-A10-A) and an oven (VH-C10-A). The column used for separation of 5 µL injected sample was an Hypersil GOLD™, maintained at 40°C. The mobile phases for separation were Milli-Q water (A) and acetonitrile (B) with each 0.1% formic acid, used at a 0.4 mL/min flow following a gradient: 0-1 min 50% B; 1-13 min linear gradient to 100% B; 13-15 min, 100% B; 15-16 min, linear gradient to 50% B; 16-20 min, 50% B. The HPLC system was coupled to a TSQ Fortis (TSQ-F-10311; ThermoFisher Scientific) using heated ESI ion source at a positive spray voltage of 3500 V, with ion transfer tube and vaporizer temperatures set at 300 °C and 350 °C, respectively. In positive SRM scan mode, the ion transitions used were: m/z 560.4→298.1, 563.4→301.1, m/z 558.4→298.1, m/z 561.4→301.1 and m/z 529.5→410.1 for derivatized cholecalciferol and cholecalciferol-d3, calcifediol, calcifediol-d3 and ergocalciferol respectively.
All peak integrations and data collecting were done on Chromeleon 7 software. Compounds were identified by their peak retention time and quantified with their peak area compared to a standard range.

Lipid quantification

10 µL sample in porpan-2-ol or 2.5 µL plasma were used for triglyceride and cholesterol quantifications using respective kits following manufacturer instructions (ref 80019 and 80106 respectively, Biolabo, Maizy, France).

Gene expression

For Aster-protein-coding gene expression in Caco-2 cells, differentiated monolayers on transwell plates were freed from apical and basolateral serum-free DMEM and directly frozen at -80 °C before RNA extraction.
RNA was extracted from mice intestinal segment mucosa and Caco-2 monolayers using 1 mL TRI Reagent®[57]. RNA concentration was assessed using Biodrop (Sci-Tec, Sandy Hook, CT, USA). One µg RNA was reverse transcript to cDNA using M-MLV 200 UI/µL (along with 0.1 M DTT and 5X First-Strand Buffer), 5 mM dNTP and random primers 0.3 µg/µL. The reaction was carried out on a Labcycler 96 gradient (SensoQuest, Göttingen, Germany). RT-qPCR were then done on 25 ng cDNA using LightCycler 480 SY Green and primers whose sequences are presented in the Key Resource Table. The amplification was processed on a LightCylcer 480 (Roche, Basel, Switzerland). Gene expression for each sample was duplicated and 18S was used as a reference gene. Results were collected on LightCycler® 480 SW 1.5.1 software and treated by the ΔCT method.

Genetic association analysis of vitamin bioavailability in a human intervention study

To assess the association between SNPs in genes encoding Aster proteins and the bioavailability of vitamin D and E, we conducted a secondary analysis of a randomized crossover intervention study in healthy adult males, designed to investigate interindividual variability in postprandial micronutrient bioavailability, as described in detail elsewhere[58–63]. Briefly, thirty-nine healthy, non-overweight, non-obese, and non-smoking adult males consumed five different test meals, with or without supplementation in selected micronutrients. Vitamin D was administered as a 5 mg dose of cholecalciferol (two vials of 100 kIU UVEDOSE; Crinex, Gentilly, France), and vitamin E as a capsule containing 67 mg (100 IU) *RRR*-α-tocopherol (Holland & Barrett, Nuneaton, UK). Postprandial chylomicrons were isolated hourly over 8 h, and micronutrient concentrations were quantified by HPLC-DAD. Bioavailability was estimated using baseline-corrected areas under the curve (AUCs) of chylomicron micronutrient concentrations from 0 to 8 h, calculated using the trapezoidal rule. Genome-wide genotyping was performed from saliva samples using HumanOmniExpress BeadChips (Illumina, CA, USA). The study was approved by the regional ethics committee (no. 2008-A01354-51, Comité de Protection des Personnes Sud Méditerranée I, Marseille, France), and all procedures complied with the Declaration of Helsinki. Written informed consent was obtained from all participants.
Gene expression of *GRAMD1A*, *GRAMD1B*, and *GRAMD1C* was first explored using the Human Protein Atlas (https://www.proteinatlas.org/), and further investigated at the single-cell level using the Gut Cell Atlas (https://www.gutcellatlas.org/). scRNA-seq data from intestinal epithelial cells were visualized using cellxgene, focusing on enterocyte populations. Expression patterns were qualitatively assessed and compared across genes, with *NPC1L1* used as a reference marker of enterocyte function. Based on these analyses, the SNP analysis was restricted to *GRAMD1B* and *GRAMD1C*.
From the 113 SNPs available on the genotyping array, SNPs with a genotype call rate below 0.95, SNPs exhibiting only a single genotype, and SNPs deviating from Hardy–Weinberg equilibrium (chi-squared test) were excluded. This initial quality control step reduced the dataset to 95 SNPs. Tag SNPs were selected using the LD TAG SNP Selection tool from the SNPinfo Web Server (HapMap European [CEU] population; https://snpinfo.niehs.nih.gov/ accessed on 14 October 2024), with an R^2 threshold of 0.80 to limit redundancy due to linkage disequilibrium, resulting in 75 SNPs retained for further analysis. SNPs were analyzed under an additive genetic model. Variants with insufficient genotype group sizes (*i.e.*, fewer than five observations in any genotypic group) were excluded to ensure stable estimation (see **Figure S3** for the SNP selection workflow). This resulted in 26 and 28 SNPs being tested for associations with vitamin E and vitamin D bioavailability, respectively. Association analyses were performed using the Wald test implemented in PLINK (v1.07). To account for potential confounding factors, analyses were conducted under three models: (a) unadjusted; (b) adjusted for age, body mass index (BMI), and fasting triglycerides; and (c) adjusted for age, BMI, fasting triglycerides, fasting cholesterol, and fasting vitamin D or E concentrations, which was considered the primary model. Multiple testing correction was performed using the Benjamini–Hochberg procedure across all association tests.

LD between SNPs was assessed using the LDmatrix tool from the LDlink platform (NIH), considering European populations. Functional annotation was performed using RegulomeDB and FORGEdb. Expression quantitative trait loci (eQTL) were explored using the GTEx portal.

QUANTIFICATION AND STATISTICAL ANALYSIS

For vitamin uptake and secretion cell experiments, n corresponds to the number of wells used for each condition, with all conditions with or without cholesterol prepared from a same batch of micelles. For mice postprandial experiment, n corresponds to the number of mice per condition. For each independent mice experiment, mice spread in 4 cages (n = 3 per cage) were randomly allocated to control or AI-3d group, in order to have 1 or 2 mice per condition per cage. All data are presented as mean ± SEM.
All statistical analysis were performed on GraphPad Prism 10.6.1 and details for tests used for each experiment are presented in figure legends. Outliers were identified using ROUT method (Q = 1%). F-test and Spearman's test were used for heteroscedasticity evaluation. When F-test was significant ($p < 0.05$), Welch's correction was applied. All data sets were following normal distribution according to Shapiro-Wilk test to test. Then, according to the data, unpaired Student's test or Two/Three-way ANOVA were applied. For Two/three-way ANOVA, Repeated Measures One-way ANOVA and Repeated Measures One-way ANOVA, Šidák's, Tukey's and Dunnett's corrections for multiple comparisons were applied according to specific test used. Significance was defined as $p < 0.05$.

ADDITIONAL RESOURCES

Clinical trial used for genetic association analysis: Study Details | NCT02100774 | Effect of Genetic Variants on Fat-soluble Vitamin Bioavailability | ClinicalTrials.gov